



Hochschule für Angewandte Wissenschaften Hamburg  
*Hamburg University of Applied Sciences*

## **Bachelorarbeit**

Lukas Müller

# **Application and enhancement of a Fortran- Software to compute panel flutter phenomena in potential flows**

*Fakultät Technik und Informatik  
Department Fahrzeugtechnik und Flugzeugbau*

*Faculty of Engineering and Computer Science  
Department of Automotive and  
Aeronautical Engineering*

**Lukas Müller**

**Application and enhancement of a  
Fotran-Software to compute panel flutter  
phenomena in potential flows**

Bachelorarbeit eingereicht im Rahmen der Bachelorprüfung

im Studiengang Flugzeugbau  
am Department Fahrzeugtechnik und Flugzeugbau  
der Fakultät Technik und Informatik  
der Hochschule für Angewandte Wissenschaften Hamburg

in Zusammenarbeit mit:  
Deutsches Zentrum für Luft- und Raumfahrt e.V.  
Institut für Aerodynamik und Strömungstechnik (IAS) | Abteilung Raumfahrzeuge  
Lilienthalplatz 7  
38108 Braunschweig

Erstprüfer/in: Prof. Dr. Hartmut Zingel  
Zweitprüfer/in : Dr. Thino Eggers

Abgabedatum: 23.02.2016

# Zusammenfassung

## Name des Studierenden

Lukas Müller

## Thema der Bachelorthesis

Weiterentwicklung und Anwendung einer Fortran-Software zur Berechnung von Panelflatterphänomenen in Potentialströmungen

## Stichworte

Panelflattern, Aeroelastik, Fortran, Linearisierte Potentialtheorie, Dynamische Instabilität, Saturn V, zeitlich variable Anströmbedingungen, Trajektorie, Machzahl, Längenverhältnis, Lagerung, Flattergrenze, Verzögerung, Grenzyklusschwingung

## Kurzzusammenfassung

Diese Arbeit umfasst eine Weiterentwicklung einer Fortran Software zur Lösung der Potentialgleichung in Kombination mit der von Kármán Plattengleichung um Berechnungen mit variablen Anströmbedingungen sowie automatische Analysen von Flutter Verhalten zu untersuchen. Mit diesem Programm wurde eine Parameterstudie durchgeführt, auf deren Basis verschiedene Trajektorien simuliert. Dabei zeigte sich, dass ein Panel beim Überqueren der Flattergrenze vom instabilen in den stabilen Bereich eine Verzögerung im Abklingverhalten aufweist. Es wurde beobachtet, dass die Verformungen vom Unterschied im dynamischen Druck gegenüber dem kritischen Wert, der Art der Anregung und der Zeit zum abfliegen der Trajektorie abhängen.

## Name of Student

Lukas Müller

## Title of the paper

Application and enhancement of a Fortran-Software to compute panel flutter phenomena in potential flows

## Keywords

Panel flutter, aeroelastic, Fortran, linearized potential flow, dynamic instability, Saturn V, time variable flow conditions, trajectory, Mach number, length-to-width ratio, aspect ratio, boundary conditions, flutter boundary, delay, limit cycle oscillation, transonic dip

## Abstract

Inside this report a Fortran software to solve the potential flow equation in combination with the von Kármán plate equation is enhanced to account for time variable flow conditions and enable automatic investigations of flutter instabilities. This program is used to conduct a parameter study on which's basis different trajectories are simulated. These computations showed a delay in the decay behaviour of the panel motion after crossing the stability boundary from the stable into the unstable regions. It was further observed that the displacements depend on the difference in the dynamic pressure above the critical values, on the initial excitation and on the time taken to travel along a trajectory.

# Contents

<b>List of Figures</b>	<b>vi</b>
<b>List of Tables</b>	<b>ix</b>
<b>Nomenclature</b>	<b>xi</b>
<b>1 Introduction</b>	<b>1</b>
1.1 Motivation . . . . .	1
1.2 Structure of the work . . . . .	3
<b>2 Literature study</b>	<b>4</b>
2.1 State of the art . . . . .	4
2.2 Parameter studies from the literature . . . . .	6
2.2.1 Panel flutter investigations . . . . .	6
2.2.2 Influence of the Mach number . . . . .	7
2.2.3 Length to width ratio . . . . .	8
2.2.4 Support conditions . . . . .	9
2.3 Launch trajecotries . . . . .	10
<b>3 Theoretical foundations</b>	<b>13</b>
3.1 Aeroelastic theory . . . . .	13
3.2 Aerodynamic theory . . . . .	19
<b>4 Computational Method</b>	<b>23</b>
4.1 Numerical implementation . . . . .	23
4.2 Time variable trajectory computation . . . . .	24
4.3 Input options . . . . .	26
4.4 Automtic solution analysis . . . . .	28

---

<b>5</b>	<b>Results</b>	<b>31</b>
5.1	Time convergence studies . . . . .	31
5.2	Validation . . . . .	34
5.3	Results of the constant flow conditions . . . . .	36
5.3.1	Effects of the Mach number . . . . .	36
5.3.2	Effects of the length-to-width ratio . . . . .	43
5.3.3	Effects of the boundary conditions . . . . .	46
5.4	Results of the time variable flow conditions . . . . .	48
5.4.1	Trajectory computations . . . . .	48
5.4.2	Trajectories traversing the stability boundary . . . . .	50
5.4.3	Trajectories traversing the transonic dip . . . . .	53
5.4.4	Influence of the difference in the dynamic pressure . . . . .	54
5.4.5	Influence of the initial excitation . . . . .	55
5.4.6	Influence of the travel time . . . . .	57
5.4.7	Influence of the panel geometry . . . . .	58
5.4.8	Trajectories affected by different participating modes . . . . .	60
<b>6</b>	<b>Summary and outlook</b>	<b>63</b>
6.1	Summary . . . . .	63
6.2	Outlook . . . . .	65
	<b>Bibliography</b>	<b>66</b>
<b>A</b>	<b>Saturn V trajectory</b>	<b>69</b>
<b>B</b>	<b>Observed mode shapes</b>	<b>70</b>
<b>C</b>	<b>Example trajectory file for the 'TAIFUN' code</b>	<b>71</b>
<b>D</b>	<b>Example input file for the 'TAIFUN' code</b>	<b>73</b>

# List of Figures

1.1	Collar's triangle of forces . . . . .	1
2.1	Typical flutter boundary showing crit. dynamic pressure for specific length to width ratio. . . . .	7
2.2	Influence of the Mach number on the amplitude of the limit cycle of the flutter oscillation. . . . .	8
2.3	Influence of the Mach number on the amplitude of the limit cycle of the flutter oscillation. . . . .	9
2.4	Influence of the support on the amplitude of the limit cycle of the flutter oscillation. . . . .	10
2.5	Influence of the support on the frequency of the limit cycle oscillation.	11
2.6	Mach number, dynamic pressure and altitude of a Saturn V trajectory.	11
3.1	Illustration of the problem modeled as a two-dimensional plate. . . .	14
4.1	Illustration of the computation scheme for constant flow conditions. . .	24
4.2	Illustration of the interpolation process of the admittance functions for time variable flow conditions. . . . .	26
4.3	Illustration of the computation process for time variable flow conditions.	27
4.4	Illustration of a damped (a), sustained (b) and excited (c) oscillation after an initial excitation in the velocity of the first natural mode with a magnitude of 0.0001. . . . .	29
4.5	Illustration of the two different methods used by the software to identify the amplitudes of the oscillation. . . . .	30
5.1	Results for the temporal resolution study of the influence on the flutter boundaries. . . . .	32
5.2	Results for the temporal resolution studies of the influence on the flutter amplitudes. . . . .	33

5.3	Stability boundary of a simply supported two-dimensional panel at low supersonic flow compared with results from Dowell and Alder . . .	35
5.4	Stability boundary of a simply supported three-dimensional panel at low supersonic flow compared with results from the literature. . . . .	36
5.5	Stability boundaries of simply supported panels with different length-to-width ratios at low supersonic flow. . . . .	37
5.6	Establishment of a higher mode by an excitation of the first natural mode. . . . .	38
5.7	Stability boundary of a two-dimensional, simply supported panel with arising flutter mode shapes. . . . .	39
5.8	Observed mode shapes of the two-dimensional panel compared to the natural modes. . . . .	39
5.9	Stability boundary of a simply supported panel with $a/b = 0.5714$ with arising flutter mode shapes. . . . .	40
5.10	Stability boundary of a simply supported panel with $a/b = 1$ with arising flutter mode shapes. . . . .	41
5.11	Stability boundary of a simply supported panel with $a/b = 1.75$ with arising flutter mode shapes. . . . .	41
5.12	LCO-amplitudes for $M = 1.2, 1.4, 1.8$ for simple supported panels with length-to-width ratios of 0 (a) and 1 (b). . . . .	43
5.13	Stability boundaries in dependency of the length-to-width ratio for different Mach numbers. . . . .	44
5.14	LCO-amplitudes for $a/b = 0, 0.5714, 1, 1.75$ of simple supported panels at (a) low- and (b) high supersonic velocities for dyn. pressures until $q/q_{crit} = 2$ . . . . .	45
5.15	Comparison of stability boundaries for clamped and pinned panels with different length-to-width ratios. . . . .	46
5.16	Comparison of stability boundaries over a range of different values of $a/b$ for clamped and pinned panels at different Mach numbers. . . . .	47
5.17	Illustration of the computed trajectories shifted by a change in the structural parameter $a^3/D$ . . . . .	49
5.18	Computation of a trajectory crossing the stability line for a two-dimensional panel. . . . .	51
5.19	Computation of a trajectory crossing the stability line for a panel with a length-to-width ratio of 1.75. . . . .	52

---

5.20	Displacements of a two-dimensional panel with a trajectory traversing through the transonic dip. . . . .	53
5.21	Trajectories with different distances from the stability boundary. . . . .	54
5.22	Computed trajectories with a distance of 25% and 50% above the dynamical pressure with a variation in the initial excitation. . . . .	56
5.23	Saturn V trajectory fitted for $a/b = 1$ crossing the flutter boundary with different travel times. . . . .	57
5.24	Trajectories beginning at similar distance in the dynamic pressure and Mach number from the stability boundary for different length-to-width ratios. . . . .	59
5.25	Trajectory crossing the stability boundary for a squared panel slightly entering the region with higher participating modes. . . . .	61
5.26	Trajectory crossing the stability boundary for a squared panel entering the region with higher participating modes. . . . .	61



# List of Tables

2.1	Overview of the theoretical models . . . . .	5
3.1	Overview of the first four modes of pinned and clamped plates . . . .	17
5.1	TRI values for the temporal resolution study of the flutter boundaries	33
5.2	TRI values for the temporal resolution study of the flutter amplitudes	34
5.3	Dominant mode shapes for pinned and clamped panels in the Mach number range from 1.2 to 1.8. . . . .	48
5.4	Initial values of the trajectories with identical travel time and dis- tances of the stability boundary in Mach number and dynamical pres- sure . . . . .	59
A.1	Time, non-dimensional time, Mach number, dynamic pressure and non-dimensional dynamic pressure of the Saturn V trajectory. . . . .	69
B.1	Overview of the observed mode shapes. . . . .	70



# Nomenclature

## Symbols

Symbol	Unit	Definition
$a$	[m]	plate length
$a_r$	[–]	generalized coordinate
$\hat{a} = \hat{w}/h$	[–]	amplitude of the plate displacement
$b$	[m]	plate width
$D$	[(kg * m <sup>2</sup> )/s <sup>2</sup> ]	plate bending stiffness
$E$	[N/m <sup>2</sup> ]	young's modulus
$F$	[–]	airy stress function
$h$	[m]	plate thickness
$h_a$	[m]	altitude
$m$	[kg/m <sup>2</sup> ]	plate mass/area
$M$	[–]	mach number
$M_n$	[–]	generalized mass
$N_x, N_y, N_{xy}$	[N/m]	in-plane stress resultants
$\Delta p$	[Pa]	aerodynamic pressure
$q_m, q_n$	[–]	generalized coordinates
$\dot{q}_m, \dot{q}_n$	[–]	generalized velocities
$Q$	[–]	generalized aerodynamic forces
$s$	[–]	time variable
$t$	[s]	time
$T$	[–]	travel time
$U$	[m/s]	fluid velocity
$w$	[m]	transverse displacement of the plate
$w/h$	[–]	normalized panel displacement
$x$	[m]	spatial coordinate in direction of the flow
$y$	[m]	spatial coordinate normal to flow direction
$z$	[m]	spatial coordinate in plate thickness direction

## Greek symbols

Symbol	Unit	Definition
$\alpha$	[–]	Fourier Transform variable
$\alpha^* = \alpha \cdot a$	[m]	Fourier Transform variable
$\gamma$	[–]	Fourier Transform variable
$\gamma^* = \gamma \cdot b$	[m]	Fourier Transform variable
$\eta = y/b$	[–]	non-dimensional coordinate
$\xi = x/a$	[–]	non-dimensional coordinate
$\lambda = \frac{\kappa M^2 a^3 p_\infty}{D}$	[–]	non-dimensional dyn. pressure
$\rho$	[kg/m <sup>3</sup> ]	density
$\sigma = \tau U/a$	[–]	time variable
$\tau = t\sqrt{\frac{D}{ma^4}}$	[–]	non-dimensional time
$\phi$	[–]	velocity potential
$\psi$	[–]	natural modes of the plate
$\omega$	[1/s]	frequency

## Superscripts

Superscript	Definition
E	= external
M	= motion dependant

## Subscripts

Subscript	Definition
LCO	= values of the limit cycle oscillation after an infinite long time
m	= in plate length direction
n	= in plate width direction
traj	= values attained by the panel flying along a trajectory
crit	= value above which the oscillation is not damped completely
$\infty$	= mean flow conditions (outside boundary layer)

---

## Abbreviations

---

<b>Abbr.</b>	<b>Definition</b>
CFD	= computational fluid dynamics
Eq.	= equation
FEM	= finite element method
Fig.	= figure
e.g.	= Example
LCO	= limit cycle oscillation
ODE	= ordinary differential equation
PDE	= partial differential equation
Ref.	= Reference
TRI	= time resolution index
Traj.	= trajectory

---

# 1 Introduction

## 1.1 Motivation

The Aeroelasticity describes interactions between the aerodynamic forces of fluids with the elastic and inertial forces of structures. These cooperating effects can engage either in a stable or an unstable system. Within the former deflections are damped until the equilibrium state is reached. For unstable systems different types of instabilities can arise. These aeroelastic problems can be illustrated within a triangle first introduced by Collar[1]. In Fig. 1.1 the shape is outlined by the three interacting forces. The arising phenomena can be included so that each aeroelastic effect is bordered by its creating forces.

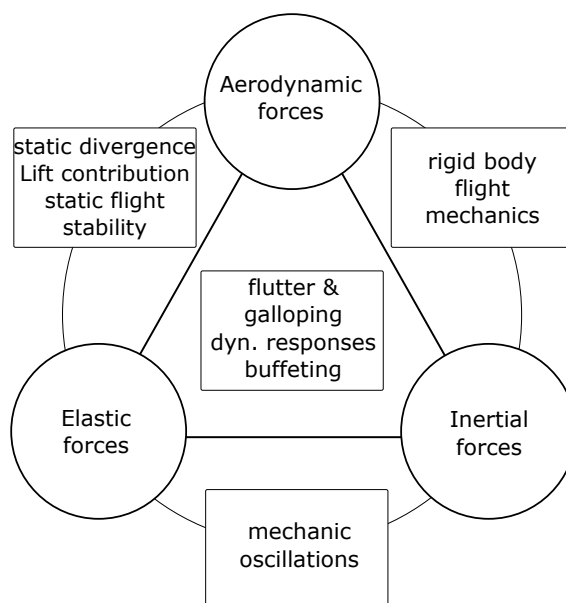


**Figure 1.1:** Collar's triangle of forces[2]

Flutter is such a phenomenon which is influenced by all three forces. It mainly arises for thin plates, exposed to a supersonic flow. Therefore it primarily is important in the design of space vehicles or supersonic aircrafts. As can be seen in figure 1.1 it is induced by an interaction between all three forces. If these inter-cooperation leads to an unstable system, the structure starts to oscillate with an increasing amplitude. For thin panels non-linearities arise due to increasing deformations of the structure. This effect acts as a damping factor and therefore limits the oscillation. In such a case the amplitude is of finite magnitude and so a limit cycle oscillation is obtained. Failure due to this effect is mainly a fatigue problem due to the finiteness of the amplitude. In some cases flutter can cause immediate damage of mounting parts or even the structure itself if the oscillation is very strong.

Panel flutter phenomena have been observed first on the German Aggregat 4 rockets in World War II. On these missiles more than 60 failures occurred due to dynamic instability of the skin[3]. The A4 was the first rocket to cross the border into space and therefore the first object strongly influenced by the effects which lead to panel flutter. With the increase of space vehicles within the space race from 1955 to 1972 the importance of panel flutter increased. Hence many investigations in these topic have been made, which focus on a variety of influencing parameters. In these studies the turbulent boundary layer has been identified as a strongly stabilizing factor. However the effect of this factor could not be investigated in detail using the methods of these times. Due to reaching the limits of the available resources and the decreasing intensity of the space race after the moonlanding in 1969, the interest in panel flutter dropped. Because of modern possibilities such as Finite Element Methods (FEM) and Computational Fluid Dynamics (CFD) the physical reality can be modelled more accurately. Due to this improvements the more complicated parameters can be investigated and hence the interest in panel flutter has been picked up again in the last years. CFD and FEM methods are even with today's possibilities very time and cost consuming. Therefore, in this work, a program based on a code from Ventres, is extended to a software which enables fast computation of panel flutter phenomena. This tool uses the full linearised potential flow theory with a nonlinear structural model and thereby possesses an advantage in computational speed. Therefore it can be used to estimate the structural responses for different values of the influencing parameters and thereby help to plan more complex investigations. With reference to space flight, panel flutter is an important factor for launch vehicles such as carrier rockets. During launch the spacecraft describes a trajectory through different altitudes attaining different magnitudes of velocity.

---

Thereby several parameters, for e.g. Mach number and dynamical pressure, change with respect to time. This leads to an interest in the effects of this time variable flow conditions on the flutter motion. Therefore the mentioned software shall be tested to include these effects within its computations.

## 1.2 Structure of the work

The structure of this thesis is intended to represent the work which was carried out to achieve the results presented in the following chapters. Therefore after a short introduction into the subject of panel flutter and the motivation of this work the conclusions gained by the literature study are pointed out. These are separated into a section about the different types of panel flutter analyses, including their development in time and a section about the outcome of past investigations in this field of study to show the influence of the different parameters. This part is followed by the theoretical foundations which shall evaluate the mathematics which are used by the applied software to compute the obtained results. Therefore the aeroelastic theory is described firstly, continued by the model which is used to simulate the aerodynamic effects on the flutter solution. The fourth chapter then begins by stating how these theories are implemented in the computer program. Further this chapter describes the modifications for the time variable computation and the added functionalities which are intended to improve the utility of this program to investigate panel flutter phenomenons. The following part gives the outcomes obtained by these computations. Firstly the carried out convergence studies are presented and afterwards the results for several varied parameters and conditions and their conclusions are stated. In the last part of this chapter the outcomes of the time variable computations are given and reviewed. The last chapter gives a discussion about the results and methodology of this work as well as an outlook of subsequent studies and further enhancements.



## 2 Literature study

The second chapter is intended to introduce the developments and outcomes of previous studies about panel flutter to the reader. Therefore an overview about the methods of investigation in this subject is given. Further the points of interest within this subject and the outcomes of previous research to several parameters, which have an effect on the flutter of the panel, are presented.

### 2.1 State of the art

Noticing the failures of the A4 rockets since 1950 investigations of panel flutter have been carried out, among others by Hayes[4] and Miles[5]. Most of these early works have been about a one-dimensional panel in a two-dimensional flow. Later studies, for example of Eisley[6] and Hedgepeth[7], regarded two-dimensional plates. In these analyses a linear structural theory was used to describe the plate, combined with a quasi-steady aerodynamic theory. They can well predict the dynamic pressure at which flutter arises and the frequency of the associated oscillation. But after passing the, so obtained, flutter boundary the increasing amplitudes lead to increasing deformations and therewith to non-linearities. However, the first type of analysis neglect these nonlinearities of the structure. Hence they can not yield reliable information about the evolution of the unstable oscillations after flutter arises. These approaches yielded good results for Mach numbers greater than  $\sqrt{2}$ , but failed to agree with experimental results of lower velocities. Such experiments have been carried out for example on the Saturn-V by Sylvester and Baker[3], who were first to show the existence of flutter within a wind tunnel test. This was followed by Sylvester et. al.[8] and by Lock and Fung[9], who showed the agreement in the higher Mach number ranges and that the results differ for lower Mach numbers. These disagreements were

assumed to be caused by the fact that the quasi-steady aerodynamics neglect the unsteadiness or memory of the fluid. This arises from the fact that the experiments and the earlier works mentioned first have shown that especially the region of Mach numbers between one and the square root of two are critical for flutter. For these lower Mach numbers the past motions of the structure and the fluid are of high importance. Therefore to investigate these velocity regions the so called full linearised inviscid potential aerodynamic theory was developed. Dowell[10] as well as Cunningham and Nelson[11] combined this approach with the linear structural theory. Dowell[12, 13] further used the full linearised theory together with a nonlinear structural theory to identify the flutter boundary for different Mach numbers and Aspect ratios as well as to compute the frequencies and amplitudes of oscillations within the unstable regions. An overview of the different theories is given in table 2.1 from McNamara and Friedmann[14]. Muhlstein et al.[15] and Muhlstein[16] have shown that the theoretical results still showed some discrepancies with the experiments for Mach numbers smaller than  $\sqrt{2}$ . They further demonstrated that in this velocity region the boundary layer is an important stabilizing factor which is not included in the previous mentioned theoretical models.

**Table 2.1:** Overview of the theoretical models

Type	Structural theory	Aerodynamic theory	Mach no.
1	Linear	Piston theory	$\sqrt{2} < M_\infty < 5$
2	Linear	Linearized potential flow	$1 < M_\infty < 5$
3	Nonlinear	Piston theory	$\sqrt{2} < M_\infty < 5$
4	Nonlinear	Linearized potential flow	$1 < M_\infty < 5$
5	Nonlinear	Euler/Navier-Stokes	all

The general solution of these analyses is to solve a system of the von-Kármán plate equation in combination with a linearized potential flow equation. This is achieved by expanding the structural deformation in its natural modes by using the Galerkin method and determining the aerodynamic forces for these modal deformations<sup>1</sup>. Alternatives to this technique are to use finite element or finite difference representations for the structure. The advantage of the modal expansion is that the first modes are mostly the active ones. Therefore the number of needed modes to describe the structural motion is much smaller than the number of elements needed

<sup>1</sup>An exact description of the fundamentals is given in chapter 2

for the finite element methods. Therefore the effort for the numerical integration is highly reduced, which was, especially due to the performance of the computers of the time of the mentioned works, an important factor. As mentioned in the introduction the amount of works about panel flutter decreased because the best outcome for the available resources of that time was reached. More recently the interest in the topic was picked up again because today possibilities allow to represent the physical effects, especially the boundary layer, very reality conform. Hence works appeared in the 21st century using modern techniques such as Computational Fluid Dynamics (CFD) and Finite Element Methods (FEM). Bendiksen and Davis[17] developed a coupled fluid structure solver based on Euler aerodynamic theory with a finite difference method for the structure. This was expanded by Gordnier and Visbal[18, 19] by using a Navier-Stokes code. Hashimoto et al.[20] used a related approach by combining a finite volume method for the fluid with a finite element method for the structure. Very recently Alder[21] compared different aerodynamic theories. He showed that non-linearities of the flow, such as compression shocks, are negligible. Thus, the more modern approaches and the modal expansion technique agree quite well. However, it was observed that the boundary layer has a strong influence within the low supersonic regions.

## 2.2 Parameter studies from the literature

### 2.2.1 Panel flutter investigations

Within the research about panel flutter, one point of interest is obviously to determine the point at which the flutter arises. Therefore the non-dimensional dynamic pressure (in the following only referenced as dynamic pressure) at which the oscillation of the plate starts to increase can be determined, as done for example by Dowell[22]. This specific pressure is called 'critical dynamic pressure'. Further investigations were carried out by Sylvester et al.[8] and Hedgepeth[7] for the panel thickness or by Cunningham and Nelson[11] and Cunningham[23] for the mass ratio. If the critical value of one of these parameters is determined over a range of variables a so called stability or flutter boundary is obtained. A typical flutter boundary is shown in Fig. 2.1, which was introduced in reference [22] and presents the critical dynamic pressure for each Mach number. Further interest has been to examine the

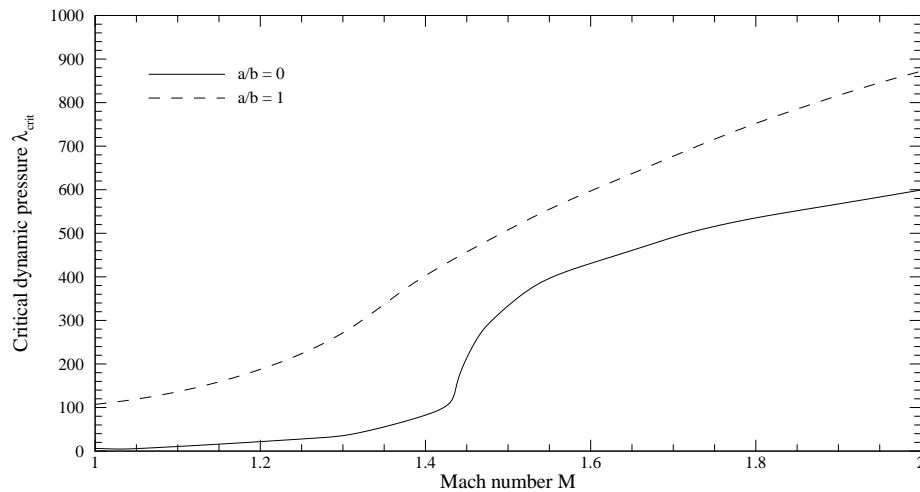


**Figure 2.1:** Typical flutter boundary showing crit. dynamic pressure for specific length to width ratio.[24]

characteristics of the flutter motion. Therefore the frequency and amplitude of the oscillation can be identified. Further the shape of the plate motion can be obtained either directly by examining the position of each point on the panel or by comparing the magnitude of the oscillation of the different modes. For each panel configuration and flow conditions a different plate motion arises. This leads to different deformations of the surface, which determine if the flutter of the panel leads to a failure of the structure. Therefore a lot of effort has been made to analyse the influences of various parameters. For a brief overview chosen effects of selected parameters are discussed in the following subsections.

### 2.2.2 Influence of the Mach number

The influence of the Mach number has already appeared in the previous section. It was said that for Mach numbers lower than  $\sqrt{2}$  the piston theory approximation is not valid. Therefore the velocity determines whether the memory of the fluid is influencing the actual panel motion or not. The Mach number further defines the duration of the capacity for remembering of the fluid. Dowell [13] showed that the influence of the memory effect approaches zero for:

$$s_{max} = \frac{M}{M - 1} \quad (2.1)$$

The motion of the panel itself is also influenced by the Mach number. The general trend is that with an increasing Mach number the critical dynamic pressure increases. This means that in the lower Mach number regions flutter is more likely to arise. An exception to this tendency is the region around  $M = 1$  which in the literature is often referenced as 'transonic dip' or 'transonic bucket'[25]. Figure 2.1 illustrates this behavior, as well as the general trend. However, the Mach number is not only a simple influencing factor in the matter of an exciting or damping parameter. It

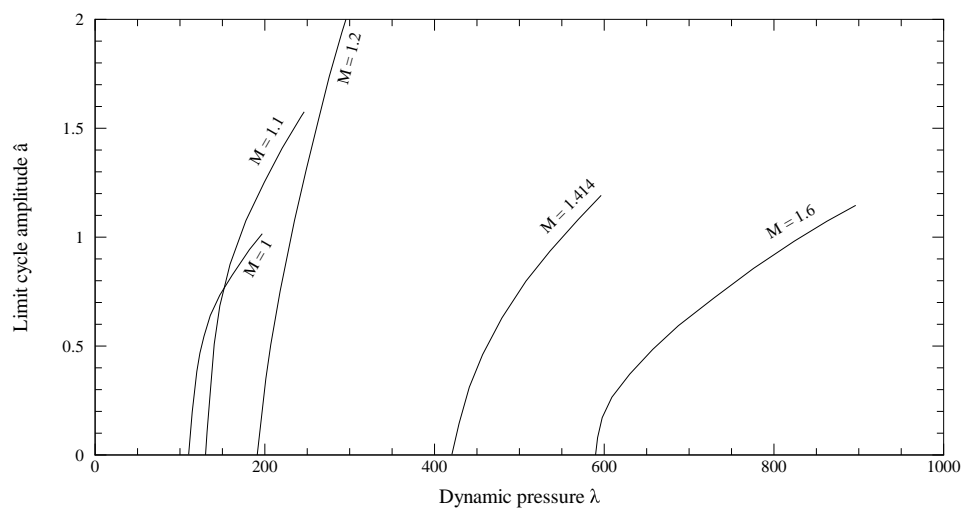


**Figure 2.2:** Influence of the mach number on the amplitude of the limit cycle of the flutter oscillation.[22]

further classifies the kind of flutter. For Mach numbers from  $M = 1$  to approximately  $M = 1.4$  a single mode is excited, whereas for higher Mach numbers higher modes contribute to the panel motion [24]. Within the subsonic speed region mainly plate divergence occurs instead of flutter. The Mach number has further an influence on the amplitude of the oscillation. This effect is shown in Fig. 2.2. The slopes of the curves for  $M > 1.2$  decrease with rising Mach numbers. This shows that at a higher velocity the amplitude of the resulting limit cycle oscillation increases slower by increasing the dynamic pressure.

### 2.2.3 Length to width ratio

A factor which describes the influence of the panel geometry is the relation between the length of the panel  $a$  (streamwise direction) to the panel width  $b$  (normal direc-

tion). The effect of the length-to-width ratio is more consistent than the influence of the Mach number. Dowell[25] showed that if the length of the panel is scaled up relatively to the width, the flutter dynamical pressure is increased as well. This can be seen in Fig. 2.1 by comparing the flutter boundary for  $a/b = 0$  and  $a/b = 1$ . Note that the former represents a two-dimensional plate. A similar relation appears for the frequency of the flutter oscillation as for higher length to width ratios it is increased and vice versa[26]. An interesting point was shown by Dowell[25]. He

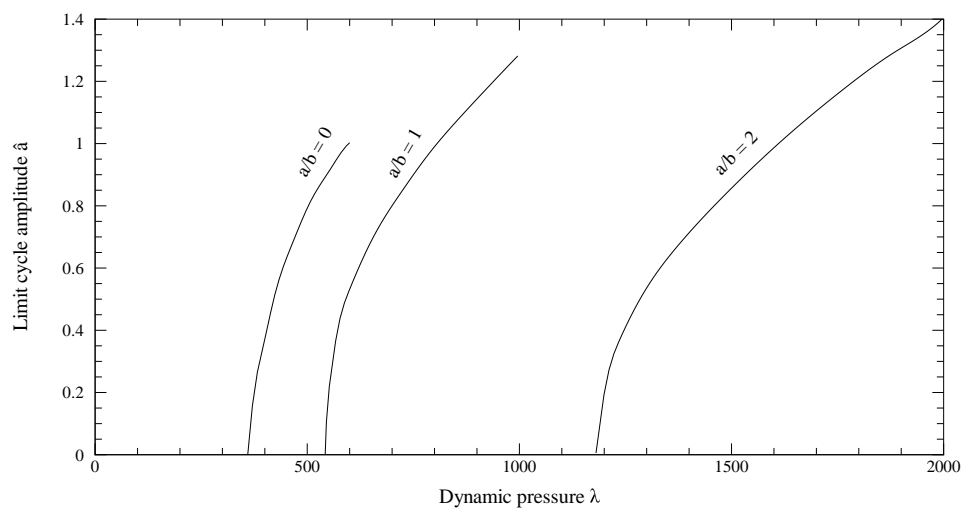


**Figure 2.3:** Influence of the mach number on the amplitude of the limit cycle of the flutter oscillation.[25]

demonstrated that panels with different length-to-width ratios behave in the same way if the dynamic pressure is increased. This is shown in Dig. 2.3. Compared with Fig. 2.2, the curves for different length to width ratios possess nearly the same slope, contrary to the curves of the different Mach numbers.

## 2.2.4 Support conditions

It is straight forward that the type of support influences the shape of the plate motion. The boundary constraints define the rate of freedom of the deformation at the plate edges and therefore the form of the oscillation. Further the support conditions influence the characteristics of the flutter oscillation. Ventres[27] showed that the general flutter behavior is the same for clamped as well as for pinned plates. However he calculated differences in the magnitude of the frequency and

amplitude of the oscillation. The effect on the amplitude of the settling limit cycle can be seen in Fig. 2.4. The curves of the clamped plates are shifted to the right

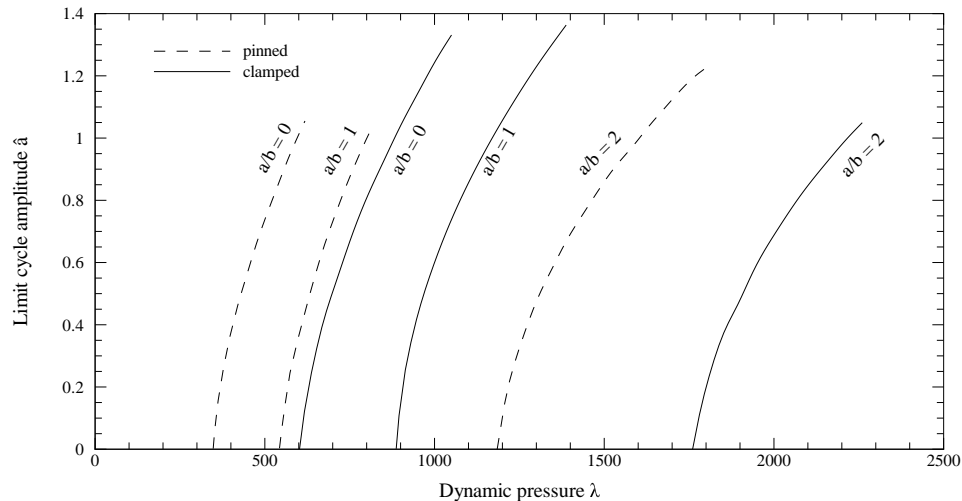


**Figure 2.4:** Influence of the support on the amplitude of the limit cycle of the flutter oscillation.[27]

compared to the curve for a pinned support. Further the illustration shows that the slopes are completely identical for pinned and clamped supports. This indicates an identical behavior for a change in dynamical pressure or in the length to width ratio. Ventres observed the same nature by comparing the frequencies of various plate geometries for pinned and clamped edge constraints. His results are illustrated in Fig. 2.5. Again the curves show no difference in their slopes but are shifted again for different boundary conditions. The clamped plates vibrate with an increased frequency compared to their pinned equivalents. This effect, as well as the panel response for lower dynamic pressures, account for the stiffening effects of the clamped edge constraints.

## 2.3 Launch trajecotries

Launch vehicles fly along specific trajectories and therefore transit different atmospheric layers. These layers exhibit different magnitudes of density and air pressure. Further such vehicles are accelerated from zero velocity to very high supersonic Mach numbers. For these reasons the structures of spacecrafts experience during

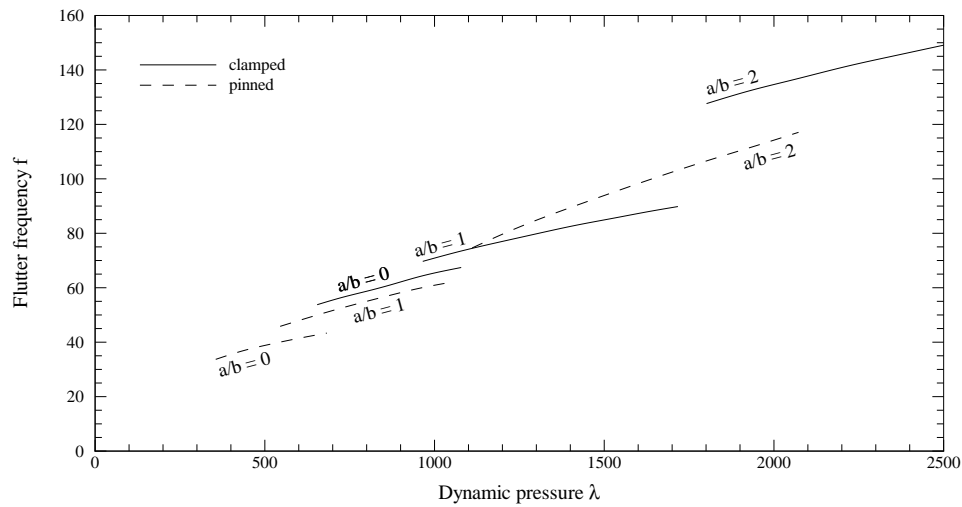


**Figure 2.5:** Influence of the support on the frequency of the limit cycle oscillation.[27]

their flight a changing influence of the different parameters with increasing time. Pinson[28] documented the launch trajectory of the Saturn V rocket which shows a good qualitative agreement with today's launch vehicles such as the Ariane V. The change in dynamic pressure, Mach number and altitude of this trajectory are shown in Fig. 2.6<sup>2</sup>. The diagram shows the magnitude of these parameters from the start

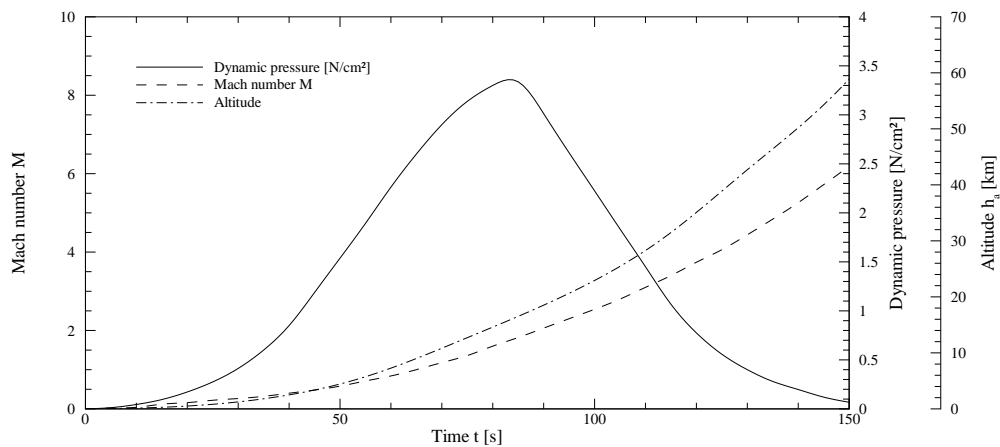


**Figure 2.6:** Mach number, dynamic pressure and altitude of a Saturn V trajectory.[28]

<sup>2</sup>A detailed table of the data from the Saturn V Trajectory is given in A including a conversion between dimensional and non-dimensional values.



to a Mach number of nearly 8, which is reached after 160 seconds. As it can be seen in the figure, the dynamic pressure increases to a maximum and then drops to zero. Therefore later points in time are uncritical and hence not important for flutter investigations. On the other side a very important point is that the critical part (with reference to the dynamic pressure) of the launch are the first minutes after the start. Regarding the curve of the Mach number, it is shown that the high magnitudes of the pressure act when the rocket is flying at small supersonic speeds. These velocity region has been identified, as mentioned earlier, as a critical range. Therefore this part of the launch can be looked at as the most dangerous and thus important to investigate.

# 3 Theoretical foundations

This chapter shall give an introduction to the equations used to model the physical foundations. Firstly, an evaluation of the aeroelastic models is given. This is continued by a discussion of the aerodynamic foundations.

## 3.1 Aeroelastic theory

The aeroelastic model is used to describe the response and motion of the panel interacting with the aerodynamic forces. It was already said in the introduction in chapter 1 that a linear structural theory cannot provide information about the oscillation after flutter arises. To describe the actual oscillation of the plate non-linearities have to be included in the theoretical model. These arise mainly through in-plane stresses which are caused by a change of the plate's length due to large out-of-plane bending. To point out the different influencing factors we will firstly consider the nonlinear equation for a one-dimensional plate which is given by:

$$D \frac{\partial^4 w}{\partial x^4} - N_x \frac{\partial^2 w}{\partial x^2} + m \frac{\partial^2 w}{\partial t^2} + \Delta p = 0 \quad (3.1)$$

This equation consists of four terms. The first one is described by the bending stiffness. The in-plane stresses which are created by the non-linearities are included in the second one. For a linear approximation this factor can be dropped. If the non-linearities shall be taken into account, the in-plan stress can be evaluated for instance for an elastic material by using Hooke's Law and assuming

$$\left(\frac{dw}{dx}\right)^2 \ll 1 \quad (3.2)$$

so that

$$N_x = E \frac{\Delta a}{a} h = \frac{Eh}{2a} \int_0^a \left( \frac{\partial w}{\partial x} \right)^2 dx \quad (3.3)$$

This shows that the stress increases with the deflection. Hence the nonlinearities are a factor which reduce the plate oscillations. The third term is defined by the mass of the plate. The last summand is an expression for the external loading, which in this case results from the aerodynamic pressure. To consider three-dimensional

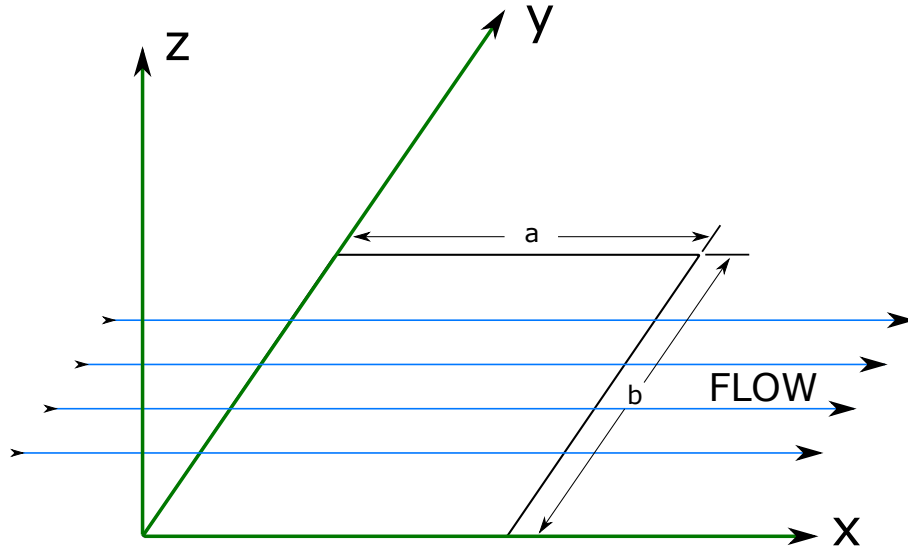


**Figure 3.1:** Illustration of the problem modeled as a two-dimensional plate.

panels as shown in Fig. 3.1, the large deformation theory of von Kármán can be used. The two-dimensional plate equation is then given by

$$D\nabla^4 w = \frac{\partial^2 F}{\partial y^2} \frac{\partial^2 w}{\partial x^2} + \frac{\partial^2 F}{\partial x^2} \frac{\partial^2 w}{\partial y^2} - 2 \frac{\partial^2 F}{\partial x \partial y} \frac{\partial^2 w}{\partial x \partial y} - m \frac{\partial^2 w}{\partial t^2} - \Delta p \quad (3.4)$$

$$\frac{\nabla^4 F}{Eh} = \left( \frac{\partial^2 w}{\partial x \partial y} \right)^2 - \left( \frac{\partial^2 w}{\partial x^2} \right) \left( \frac{\partial^2 w}{\partial y^2} \right) \quad (3.5)$$

The in-plane stresses are included in the so called airy stress potential function  $F$  in the following form:

$$\begin{aligned} N_x &= \frac{\partial^2 F}{\partial y^2} \\ N_y &= \frac{\partial^2 F}{\partial x^2} \\ N_{xy} &= -\frac{\partial^2 F}{\partial x \partial y} \end{aligned} \quad (3.6)$$

if  $F$  satisfies the in-plane equilibrium equations

$$\begin{aligned} \frac{\partial N_x}{\partial x} + \frac{\partial N_{xy}}{\partial y} &= 0 \\ \frac{\partial N_y}{\partial y} + \frac{\partial N_{xy}}{\partial x} &= 0 \end{aligned} \quad (3.7)$$

the in-plane stresses can be evaluated further into strains and deformation of the structure. As this is not a crucial factor for this work, this will not be considered here but the reader can be referred to the appendix of reference [24]. To obtain a solution of equations (3.4) and (3.5) the modal expansion technique can be used. Therefore the deformations  $w$  as well as the airy stress function  $F$  can be expanded in terms of the natural modes of the structure:

$$w = \sum_m q_m \psi_m(x) \psi_n(y) \quad (3.8)$$

$$F = \sum_r a_r \phi_r(x, y) \quad (3.9)$$

For a pinned plate these modes are composed of two sinusoidal waves, one in the direction of the plate length  $\psi_m$  and one in the direction of the plate width  $\psi_n$ :

$$\psi_m = \sin\left(\frac{m\pi x}{a}\right) \quad (3.10)$$

$$\psi_n = \sin\left(\frac{n\pi y}{b}\right) \quad (3.11)$$

The equations for a clamped plate is a little more complicated due to its boundary conditions:

$$\psi_m = \cos\left((m-1)\pi\frac{x}{a}\right) - \cos\left((m+1)\pi\frac{x}{a}\right) \quad (3.12)$$

$$\psi_n = \cos\left((n-1)\pi\frac{y}{b}\right) - \cos\left((n+1)\pi\frac{y}{b}\right) \quad (3.13)$$

In equations (3.12) to (3.11)  $m$  and  $n$  represent the number of the mode in the length or in the width direction and therefore determine the shape of the mode, for e.g. half a sinusoidal cycle or a full sinusoidal cycle. The first four normal modes of a pinned and a clamped plate are shown in table B.1.

These natural modes have to satisfy the same boundary conditions as  $w$  and so the following restraints must hold with respect to mass:

$$\begin{aligned} \int m\psi_m\psi_n dx &= M_n & \text{for } m = n \\ \int m\psi_m\psi_n dx &= 0 & \text{for } m \neq n \end{aligned} \quad (3.14)$$

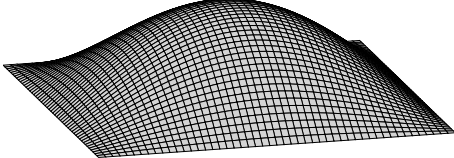
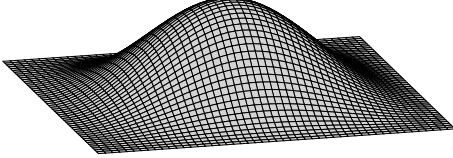
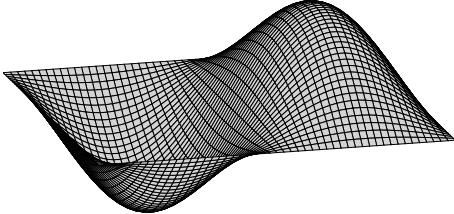
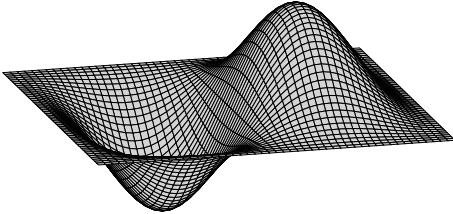
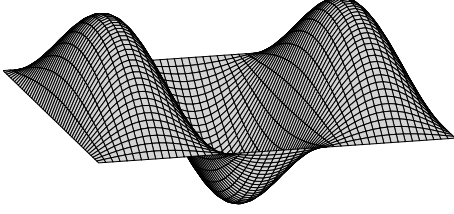
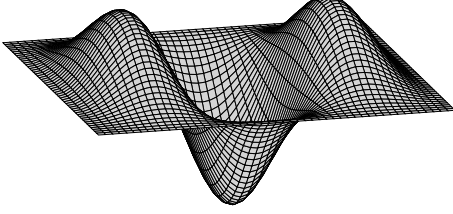
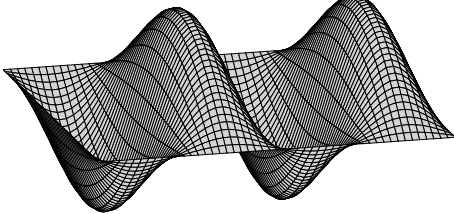
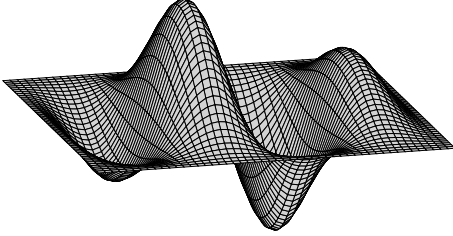
and with respect to stiffness:

$$\begin{aligned} \int D \frac{d^2\psi_m}{dx^2} \frac{d^2\psi_n}{dx^2} dx &= \omega_n^2 M_n & \text{for } m = n \\ \int D \frac{d^2\psi_m}{dx^2} \frac{d^2\psi_n}{dx^2} dx &= 0 & \text{for } m \neq n \end{aligned} \quad (3.15)$$

For the non-linear in-plane stresses the equations

$$\begin{aligned} N_x = N_{xy} &= 0 & \text{on } x = 0, a \\ N_y = N_{xy} &= 0 & \text{on } x = 0, b \end{aligned} \quad (3.16)$$

**Table 3.1:** Overview of the first four modes of pinned and clamped plates

$m/n$	pinned	clamped
1/1		
2/1		
3/1		
4/1		

must hold as well as the out-of-plane boundary conditions

$$\begin{aligned}
 w &= 0 \\
 \frac{\partial w}{\partial x} &= 0 \quad \text{on } x = 0, a \\
 \frac{\partial w}{\partial y} &= 0 \quad \text{on } x = 0, b
 \end{aligned} \tag{3.17}$$

for a clamped plate and for a pinned plate additional

$$\begin{aligned}
 \frac{\partial \dot{w}}{\partial x} &= 0 \\
 \frac{\partial \dot{w}}{\partial y} &= 0
 \end{aligned} \tag{3.18}$$

If all conditions are satisfied the following system of equations is obtained according to the Galerkin method:

$$\sum_m q_m K_{mn} + \ddot{q}_m M_{mn} + Q_n = \sum_r \sum_m a_r q_m L_{rnm} \tag{3.19}$$

$$\sum_r a_r A_{rs} = \sum_l \sum_m q_l q_m B_{lms} \tag{3.20}$$

where

$$B_{lms} \equiv \iint \left[ \frac{\partial^2 \phi_l}{\partial x \partial y} \frac{\partial^2 \psi_m}{\partial x \partial y} - \frac{\partial^2 \phi_l}{\partial x^2} \frac{\partial^2 \psi_m}{\partial y^2} \right] \phi_s dx dy \tag{3.21}$$

$$L_{rnm} \equiv \iint \left[ \frac{\partial^2 \phi_r}{\partial y^2} \frac{\partial^2 \psi_m}{\partial x^2} + \frac{\partial^2 \phi_r}{\partial x^2} \frac{\partial^2 \psi_m}{\partial y^2} - 2 \frac{\partial^2 \phi_r}{\partial x \partial y} \frac{\partial^2 \psi_m}{\partial x \partial y} \right] \psi_n dx dy$$

Note that the terms included in equations (3.19) and (3.20) again represent some of the influencing factors like the mass within

$$M_{mn} = \iint m \psi_m \psi_n dx dy \tag{3.22}$$

and the stiffness within

$$K_{mn} \equiv \iint D \nabla^4 \psi_m \psi_n dx dy \tag{3.23}$$

Further the in-plane stresses are included in:

$$A_{rs} \equiv \int \int \frac{\nabla^4 \phi_r}{Eh} \phi_s dx dy \quad (3.24)$$

The aerodynamic effects are represented by

$$Q_n \equiv \int \int \Delta p \psi_n dx dy \quad (3.25)$$

and will be evaluated in detail in chapter 3.2.

## 3.2 Aerodynamic theory

It was already mentioned that the external loadings are created by the aerodynamic pressure. Therefore it is essential to evaluate the aerodynamic effects in a very detailed way. The pressure can arise out of two reasons, either from a external source, for e.g. a disturbance in the flow, or created by the motion of the plate itself. Hence the total pressure is obtained by a superposition of those two pressures:

$$\Delta p = \Delta p^E + \Delta p^M \quad (3.26)$$

Whereas the former has to be taken from experiments, the latter can be evaluated. For the fully linearized potential flow theory the pressure can be evaluated starting from the equation for a potential flow in the form, given by Garrick [2]:

$$\nabla^2 \phi = \frac{1}{a_\infty^2} \frac{D_C^2 \phi}{Dt^2} \quad (3.27)$$

Performing a Galilean transformation, the equation which describes the flow field in the full linearized, inviscid potential theory [13] is obtained as:

$$\nabla^2 \phi - \frac{1}{a_\infty^2} \left[ \frac{\partial}{\partial t} + U_\infty \frac{\partial}{\partial x} \right]^2 \phi = 0 \quad (3.28)$$

Satisfying the boundary condition

$$\left. \frac{\partial \phi}{\partial z} \right|_{z=0} = \left[ \frac{\partial}{\partial t} + U_\infty \frac{\partial}{\partial x} \right] w = f'' \quad (3.29)$$



as well as an outward radiation conditions for  $z \rightarrow \infty$ . This equation, obtained by the Galilean transformation, describes the velocity potential within a moving coordinate system. To solve the partial differential equation (PDE) for the velocity potential, this can be evaluated with respect to time employing a Laplace-Transformation for  $t$  and a Fourier-Transformation for the spatial variables  $x$  and  $y$ , as it was performed in reference [13]. Therewith the PDE is transformed to an ordinary differential equation (ODE). Solving this ODE with respect to the potential  $\phi$  and applying the inverse Laplace-Transformation with respect to  $t$  yields:

$$\phi^*(\gamma, \alpha, z = 0, t) = -\alpha \int_0^t f^*(\gamma, \alpha, \tau) \cdot \exp[-iMa\alpha(t - \tau)] \cdot J_0[\sqrt{\alpha^2 + \gamma^2} \cdot a(t - \tau)] d\tau \quad (3.30)$$

of the velocity potential. This is substituted into the Bernoulli formula

$$p = -\rho \left[ \frac{\partial \phi}{\partial t} + U \frac{\partial \phi}{\partial x} \right] \quad (3.31)$$

which relates the pressure  $p$  and the potential  $\phi$ . For the solution process in this work only the inverse-transformations are not needed and hence not explicitly derived but only shown for the sake of completeness. The motion depended pressure  $\Delta p^M$  can be expressed [24] as

$$\Delta p^M(x, t) = \rho_\infty U_\infty^2 \left\{ \frac{1}{M} \left[ \frac{\partial w}{\partial x} + \frac{1}{U_\infty} \frac{\partial w}{\partial t} \right] + \int_0^t \int_0^a A(x - \xi, t - \tau) \cdot \left[ \frac{\partial w}{\partial \xi} + \frac{1}{U_\infty} \frac{\partial w}{\partial \tau} \right] d\xi d\tau \right\} \quad (3.32)$$

The simplest way to approximate the aerodynamic effects is to neglect the spatial- and temporal memory of the fluid. Because only the second term accounts for this memory it can easily be dropped to give the equation for the piston theory.

$$\Delta p^M = \frac{\rho_\infty U_\infty^2}{M} \left[ \frac{\partial w}{\partial x} + \frac{1}{U_\infty} \frac{\partial w}{\partial t} \right] \quad (3.33)$$

As mentioned earlier this approximation is not valid for Mach numbers smaller than  $\sqrt{2}$ , for this reason the potential flow theory uses the full equation (3.32), including the second term and hence incorporating the memory effects. The generalized aerodynamic forces, needed for the solution process used in the current work,

can be obtained starting from the definition of the generalized motion dependent pressure[24]:

$$Q_{mn} \equiv \iint \frac{\Delta p_m}{\rho_\infty U_\infty^2} \psi_m dx dy \quad (3.34)$$

Substituting the modal expansion

$$w = \sum_m \sum_n q_{mn} \psi_m(x) \psi_n(y) \quad (3.35)$$

into equation (3.34) and then performing the integrals over  $x$  and  $y$  before using a Fourier Transform yields the generalized aerodynamic forces:

$$Q_{mnpq} = q_m(s) S_{mnpq} + \dot{q}_m(s) D_{mnpq} + \int_0^s [q_m(\sigma) H_{mnpq}(s - \sigma) + \dot{q}_m(\sigma) I_{mnpq}(s - \sigma)] d\sigma \quad (3.36)$$

where

$$S_{mnpq} \equiv \frac{1}{M} \int \frac{d\psi_m(\xi)}{dx} \psi_p(\xi) \int \psi_n(\eta) \psi_q(\eta) dx dy \quad (3.37)$$

$$D_{mnpq} \equiv \frac{1}{M} \int \psi_m(\xi) \psi_p(\xi) \int \psi_n(\eta) \psi_q(\eta) dx dy \quad (3.38)$$

are the equivalent factors to piston theory and

$$H_{mnpq}(s) \equiv -\frac{1}{4\pi^2 M^2} \int_{-\infty}^{+\infty} \int_{-\infty}^{+\infty} G_{mnpq} i\alpha^* \sqrt{\alpha^{*2} + \gamma^{*2} \frac{a^2}{b}} \cdot \exp[-i\alpha^* s] J_1 \left[ \sqrt{\alpha^{*2} + \gamma^{*2} \frac{a^2}{b}} \frac{s}{M} \right] d\alpha^* d\gamma^* \quad (3.39)$$

$$I_{mnpq}(s) \equiv -\frac{1}{4\pi^2 M^2} \int_{-\infty}^{+\infty} \int_{-\infty}^{+\infty} G_{mnpq} \sqrt{\alpha^{*2} + \gamma^{*2} \frac{a^2}{b}} \cdot \exp[-i\alpha^* s] J_1 \left[ \sqrt{\alpha^{*2} + \gamma^{*2} \frac{a^2}{b}} \frac{s}{M} \right] d\alpha^* d\gamma^* \quad (3.40)$$

are the terms which contribute the memory effects and are called 'admittance functions'. Where

$$G_{mnpq} \equiv \int_0^1 \psi_m(\xi) \cdot \exp[-i\alpha^*\xi] d\xi \int_0^1 \psi_p(\xi) \cdot \exp[i\alpha^*\xi] d\xi \cdot \int_0^1 \psi_n(\eta) \cdot \exp[-i\gamma^*\eta] d\eta \int_0^1 \psi_q(\eta) \cdot \exp[i\gamma^*\eta] d\eta \quad (3.41)$$

is only defined by geometric conditions. An important point to keep in mind is that only these are the difference to the generalized forces of the piston theory and account for the past deformations and velocities of the panel.

# 4 Computational Method

The following sections describe the computation process of the 'Temporal Adapting Integrator for Flutter Understanding' in the following called 'TAIFUN'. In the first part the computation steps, which are used to solve the equations given in chapter 3, are explained. Because the software is based on a code from Ventres[27], not each computation step is described but the principal calculations and their interrelations are evaluated, so that the reader gets an overview about the functionality of the program and can understand the modifications for the time variable flow conditions which are introduced in chapter 4.2. Further the possible input settings for the user are described. The last section illustrates the integrated functions for automatic solution analysis and investigations.

## 4.1 Numerical implementation

To determine the solution of the aeroelastic system given by Eq. (3.4) and (3.5) a time integration method is applied to solve for the generalized coordinates. This integration is accomplished by an explicit multi-step method known as the Adams-Bashforth method. Therefore the system of equations (3.19) and (3.20) is solved. Here the influence of the aerodynamic effects are contributed through their generalized forces  $Q_n$  given by factor (3.25). For the linearized potential flow theory the generalized forces are obtained by the modal expansion of the governing field equation of the velocity potential (3.28) as described in chapter 3.2. Therefore equation (3.36) is solved. For constant flow conditions the solutions of the terms (3.37) to (3.41) do not change from the first time step onwards. Hence they can be calculated once and for all. The factors  $S$  and  $D$  have to be multiplied by the actual deformation and velocity of the plate. As stated before, the integrals yield the memory

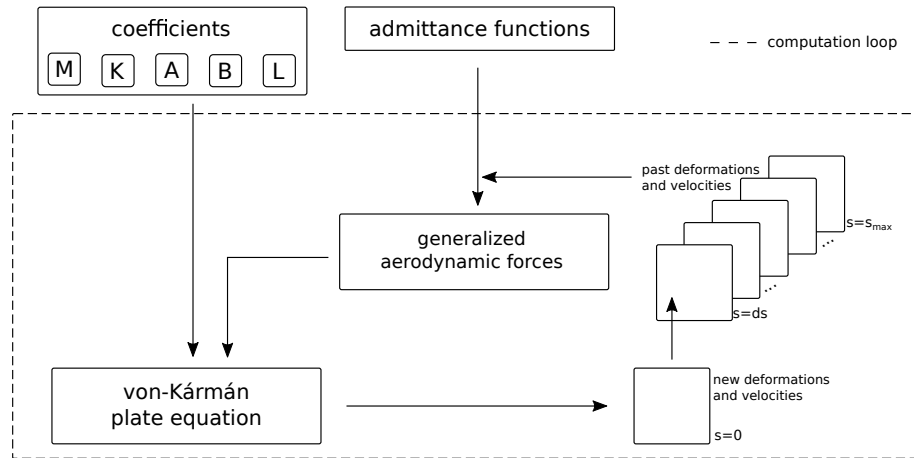


**Figure 4.1:** Illustration of the computation scheme for constant flow conditions.

effects. Therefore the admittance functions are multiplied by the past deformations  $q$  and velocities  $\dot{q}$ . This is done for each past time step  $ds$  from the first (previous) point of time  $s = 0$  until  $s = s_{max}$  which is estimated from equation (2.1). A point which has to be kept in mind is that  $ds$  differs from  $d\tau$  with a conversion of the following form:

$$ds = d\tau \cdot \sqrt{\frac{\lambda}{\mu}} \quad (4.1)$$

The sum of all those products yields the generalized force for one specific mode. If these and the other terms of (3.19) and (3.20) are determined, the system of equations can be solved. An overview of the relations is given in Fig. 4.1. This yields the deformations and velocities of the next time step. The actual deformations and velocities are stored as the new previous values and the next computation step begins.

## 4.2 Time variable trajectory computation

In chapter 2.3 it was shown that for launch trajectories some influencing parameters change with respect to time. These variables have to be determined for every time step. Therefore an input file containing a table with values of the time dependent parameters for different points of time is read by the program. An example of such a file is given in the appendix C. Because it is unlikely that the given time points are conform with the chosen time step size, a linear interpolation between the given values was added to the software. This is done at the beginning of each

time step to ensure that all factors are calculated with the actual Mach number and dynamic pressure. Therefore the current point of time is determined and compared with the values from the trajectory file. The higher and lower values are taken as nodes  $P_0(x_0, y_0)$  and  $P_1(x_1, y_1)$  between which the interpolation is carried out and the actual value is obtained by the equation:

$$y = y_0 + (y_1 - y_0) \frac{x - x_0}{x_1 - x_0} \quad (4.2)$$

This is done for the Mach number  $M$  as well as for the non-dimensional dynamic pressure  $\lambda$ . Regarding equations 3.36 to 3.41 it can be seen that the factors  $S$ ,  $D$ ,  $H$ , and  $I$  depend on the Mach number. Hence their calculation has to be carried out for each time step and therefore is included in the computation loop of the program. Including the admittance functions  $H$  and  $I$  into the time variable computation is a relatively complicated subject. On the one side, not only the Mach number changes for the calculation but because of the conversion factor between  $s$  and  $\tau$  also the time step size  $ds$  of the admittance functions and the number of time steps to reach  $s_{max}$  is different for each point in time. On the other side, the admittance functions express the ability of the past deformations and velocities to influence the actual deformation. Each past motion experienced different flow conditions, which means that each past state is 'remembered' in the magnitude defined by the values of the constellation of that time. Hence the values which are multiplied with the deformation and velocity of a specific point of time have to be calculated again for each next step because for every next computation loop the state lies back one time step further. It follows that the influence of this specific state is different for each time step until it has no influence anymore. Therefore an array is introduced which assigns a value of  $ds$ ,  $M$ ,  $\lambda$ ,  $s_{max}$  and  $\tau$  to each 'memory state'. Figure 4.2 illustrates the process to determine the admittance functions for time variable computations. So the admittance function of that time can be evaluated and therewith the influence determined, which the state has on the coming plate motion. Further the admittance function for each given point of time in the trajectory input file is calculated in advance of the computation loop. This enables to interpolate between these reference functions within the computation loop. To implement this, the program recalls the saved value of  $\tau$  from the memory array for a specific past state and determines

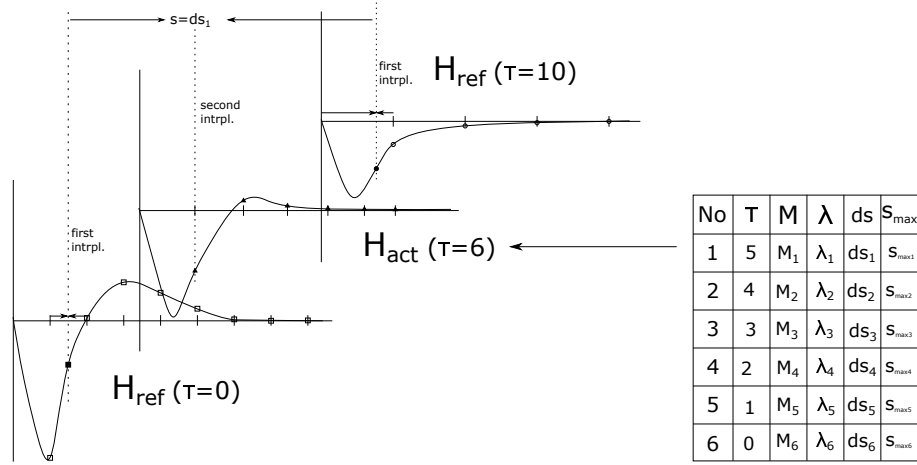


**Figure 4.2:** Illustration of the interpolation process of the admittance functions for time variable flow conditions.

the lower and higher given points of time from the input trajectory. Then a double Lagrangian interpolation of the form

$$f_n(x) = \sum_{i=0}^n \prod_{j=0; j \neq i}^n \frac{x - x_j}{x_i - x_j} \cdot f(x_i) \quad (4.3)$$

is applied to calculate the associated values of the admittance functions. The first interpolation is carried out to obtain the compatible values of the reference admittance functions. This is needed because at each time a different conversion factor between  $s$  and  $\tau$  has to be used due to the change in dynamic pressure and altitude. Therefore the needed value of the reference admittance functions for the accurate point of time is interpolated between the available values from the pre-calculation. Afterwards between these values the actual values of  $H$  and  $I$  are interpolated and then multiplied by the associated past deformation or velocity. The two interpolation steps can also be seen in Fig. 4.2, whereas the Fig. 4.3 shows the changes compared to the computation with constant flow conditions.

### 4.3 Input options

To enable a user-friendly and fast execution of the program all settings and adjustments can be written into an input file, which is handed over to the program as an argument when the execution command is invoked. This file contains parameters which can be set by the user and is parsed by the software directly after the start.

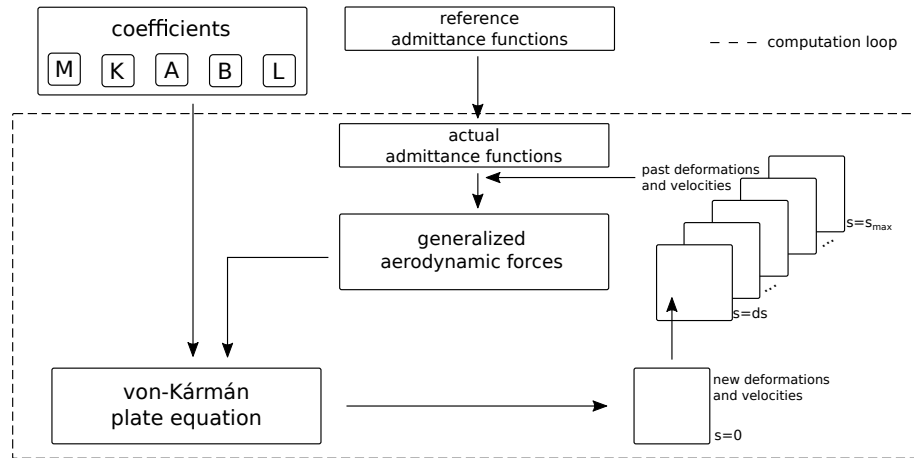


**Figure 4.3:** Illustration of the computation process for time variable flow conditions.

The program searches for all possible input instructions one after another. Thereby it reads the statements line by line until the identifier of the actual searched parameter is found. The identifiers of the input statements have to be entered correctly. A template of an input file including all identifiers for each possible statement with explanations is given in appendix D. If the correct identifier was found, the program splits the line including the statement after the last symbol of the identifier. Then the tail is stored as the chosen value of the actual parameter. The entered value can be separated by an equality sign or a colon and a chosen number of blanks. If the value is entered correctly according to the type of the parameter (integer, real, boolean, ...) it is stored and the software continues to scan the file for additional occurrences of the same identifier. To enable fast input adjustments the program uses the last (closest to the end of the file) appearance of a parameter. Thereby it can distinguish if the identifier of a distinct parameter is used as an identification mark or as a value of another input statement (i.e. as an iteration or adjustment parameter). If the correct identifier was not found the program uses a standard value as input and continues with the next parameter. To monitor the found input values as well as the calculation process, a computation-log can be written into a file and to the terminal. Herein the successfully received values of the inputs as well as the not or incorrect given parameters with their instead used standard values are stated. Further the actual progress of the computation steps is shown.

The software can calculate the flutter motion for a chosen number of points along the plate length. Further via Eq. (3.35) the modal solution can be transformed in an arbitrary set of x- and y-coordinates. This can be used to create a grid consisting



of a chosen number of points in x- and y-direction which can be used to simulate the motion of the plate surface. The results are plotted into a data file and can be viewed by any post processing tool such as Tecplot or Gnuplot or copied to a spreadsheet analysis. Because the size of the file containing the solutions increases drastically if the grid for the surface deformations is plotted, this output can be limited to a number of small periods with an up-scaled time step increment. These solutions can be computed for various constellations of the parameters which effect panel flutter. Therefore the values of the Mach number, Length-to-width ratio dynamic pressure and others<sup>1</sup> can be chosen by the user. The input of these variables can be either in a non-dimensional form or using SI units. Further the calculation mode can be switched between linear(according to type 1 and 2 of table 2.1) and nonlinear (type 3 to 5) and the aerodynamic theory can be selected between the linearized potential theory, the piston theory or no aerodynamic theory at all. To simulate a perturbation in the flow the initial displacement and velocity of each mode can be specified in the input file.

## 4.4 Automtic solution analysis

The software computes the solution by an integration in time and thus only solutions for distinct points with a single specified set of parameter values can be calculated. Therefore the stability boundary can only be identified by an iterative approach to the critical value. For a faster and more user-friendly execution of this method an automatic iteration mode as well as an automatic analysis mode was integrated in the program code. Within the iteration mode a parameter can be selected, which is iterated from a start value until a specified limit with a chosen increment. This functionality enables easy investigations of the flutter behavior due to a change of a specific parameter. The automatic analysis is intended to facilitate the identification of the flutter boundary. This feature utilizes the fact that the damping behavior of the aerolelastic system can be characterized by the increase or decay of an arbitrary excitation. Further the damping is proportional to the logarithmic decrement of the structural oscillation. Due to this relations the software can automatically

---

<sup>1</sup>A list of all adjustable parameters can be taken from the template input file in appendix D.

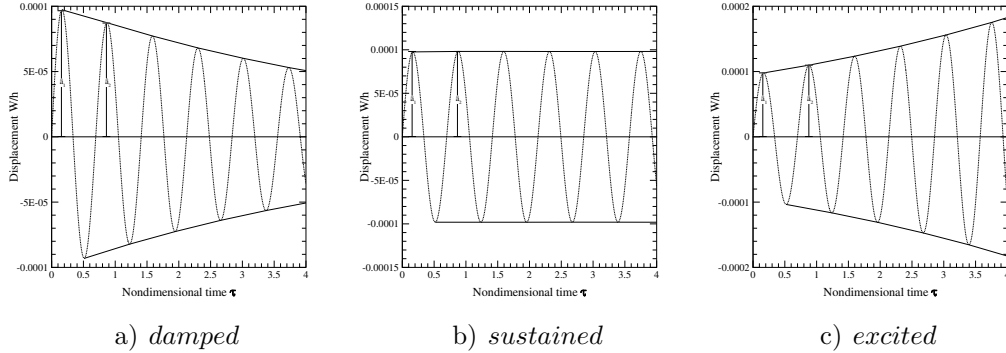


**Figure 4.4:** Illustration of a damped (a), sustained (b) and excited (c) oscillation after an initial excitation in the velocity of the first natural mode with a magnitude of 0.0001.

distinguish between a damped, excited or sustained oscillations by computing the log. decrement which is defined as:

$$\Lambda = \ln \frac{\hat{a}_1}{\hat{a}_2} \quad (4.4)$$

Given values of an 'adjustment' parameter which lead to an excited and a damped oscillation, the software is able to iterate between these limits until the log. decrement becomes zero and the critical value of the adjustment parameter is found. Fig. 4.4 presents a damped, excited and sustained oscillation. To compute a solution of Eq. 4.4 the magnitudes of a time-series of amplitudes is required and thus the program has to identify the extrema of the panel displacements. To accomplish this, the file containing the solution is processed line by line and the maxima and minima of the oscillation are determined. This can be done using two different methods. On the one hand, by comparing the slopes and identifying the extreme values through a change in the slope of the plate displacements (Fig. 4.5 a). To limit errors due to numerical outliers the number of slopes which have to be in agreement at both sides of an extreme value can be chosen. The second method is a direct comparison of the actual magnitudes of the deformations (4.5 b). Thereby the software reads each line of the solution file. If the actual deformation is greater or smaller (depending on the position above or below x-axis) than the previous values it is stored as a extrema. When the process crosses the x-axis the current extreme value is saved as a maximum or a minimum. To prevent that each numerical outlier is recognized as an extreme value the current value with the highest magnitude is compared with the

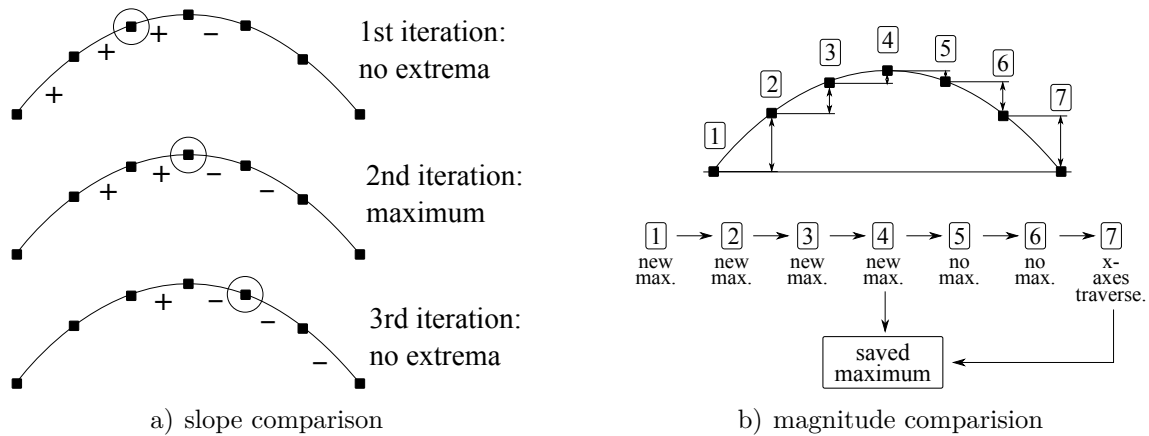


**Figure 4.5:** Illustration of the two different methods used by the software to identify the amplitudes of the oscillation.

last saved minimum or maximum and only saved if its magnitude is higher than a specific fraction of the previous. Which of the two variants yields the higher success depends on the analysed oscillation. However, during the calculations of this work the latter showed a slightly improved behaviour for oscillations which are more difficult to distinguish. If the amplitudes are determined three attempts of analysis are carried out. The first probes if all local decrements (log. decrements between each pair of maxima) are negative, positive or zero<sup>2</sup>. If this fails the second step is to determine if the main fraction of all local decrements is negative, positive or zero. In the last try the global logarithmic decrement is computed and compared with the growth (difference between the mean value of the first and second half of the amplitudes) of the oscillation. The three different attempts have been introduced because identifying the damping of the system may be complicated for example due to interferences of more than one harmonic oscillation. Further higher harmonic influences or numerical errors may cause local peaks which falsify the identified damping behavior. Due to the three analysis steps and the possibilities of input adjustments, the automatic analysis proved successful for the most of the constellations of parameters. However for Mach numbers around  $M = 1.4$  due to a raised complexity of the results created by contributions of the higher modes the analysis failed repeatedly. A more detailed discussion of these effects is deferred to chapter 5.3.1.

<sup>2</sup>The allowed deviation from zero can be set in the input file.

# 5 Results

In the following sections the obtained results are presented for the time variable flow conditions as well as for the steady computations. Further the outcomes are compared to the results from the literature and discussed. A temporal resolution study is conducted in order to determine an appropriate time step size with respect to different flutter cases. This is followed by presenting the results for time invariant parameters and comparing these with the literature. The outcomes of the newly integrated time variable computation are given in the third and last part.

## 5.1 Time convergence studies

In various previous investigations[19],[29] of panel flutter with coupled fluid structure solvers it was shown that the time step size can have a strong impact on the results. Therefore a time resolution study was made for four different parameter settings. To account for low supersonic Mach numbers as well as for higher values the time step size  $d\tau$  was varied from 0.01 to approx. 0.0002 for  $M = 1.2$  and  $M = 1.8$ . For both Mach numbers the time convergence was analysed for a two-dimensional plate ( $a/b = 0$ ) and a square plate ( $a/b = 1$ ). The results of the resolution study are presented in Fig. 5.1. The given values represent the flutter boundary of the different parameters normalized to the smallest value of  $d\tau$ . It can be seen that the higher Mach numbers are more influenced by the time step size than the results at  $M = 1.2$ . Further the illustration shows that the two-dimensional plate is less sensitive to the time resolution than the square plate. This leads to the conclusion that more caution has to be made for higher Mach numbers and length to width ratios. A reason for this behaviour could be that for higher values of these two parameters the panel flutters with a much higher frequency and hence numerical

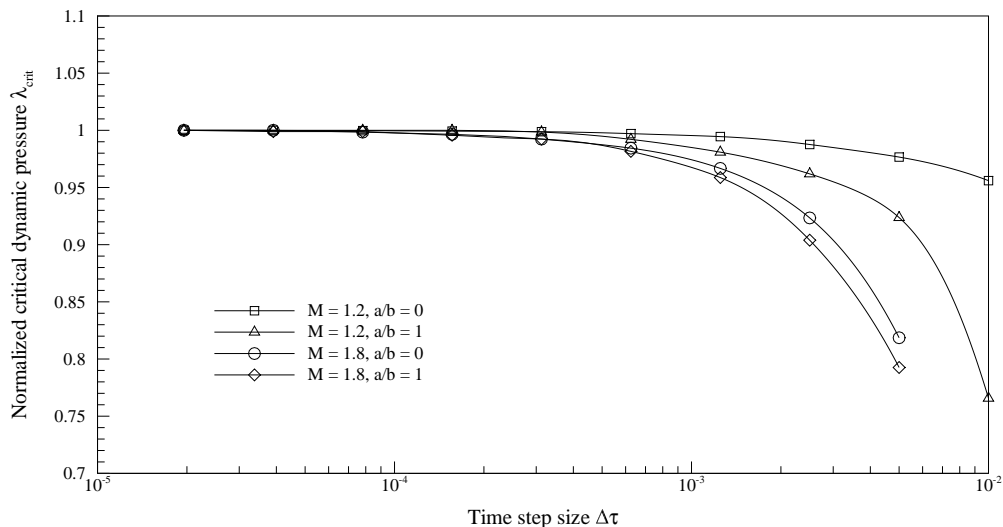


**Figure 5.1:** Results for the temporal resolution study of the influence on the flutter boundaries.

errors can have a greater influence. Further for these conditions the panel begins to flutter at larger dynamic pressures. Due to the conversion between  $d\tau$  and  $ds$  through equation (4.1) such high values of  $\lambda$  lead to a coarser time step size of the admittance functions. Another point which can be observed from Fig. 5.1 is that the curves show a decrease of the identified flutter boundary for higher time step sizes. Hence using a coarser temporal resolution would still be a conservative approximation. In order to facilitate a quantitative judgement of the results a time resolution index (TRI) is calculated accordingly to the Grid Convergence Index of a Richardson-Extrapolation as described in Ref. [30]. This expresses the deviation of a value to the result of the next finer time step and is computed by

$$TRI_{i-(i-1)} = \frac{F_s |\varepsilon| r^p}{r^p - 1} \quad (5.1)$$

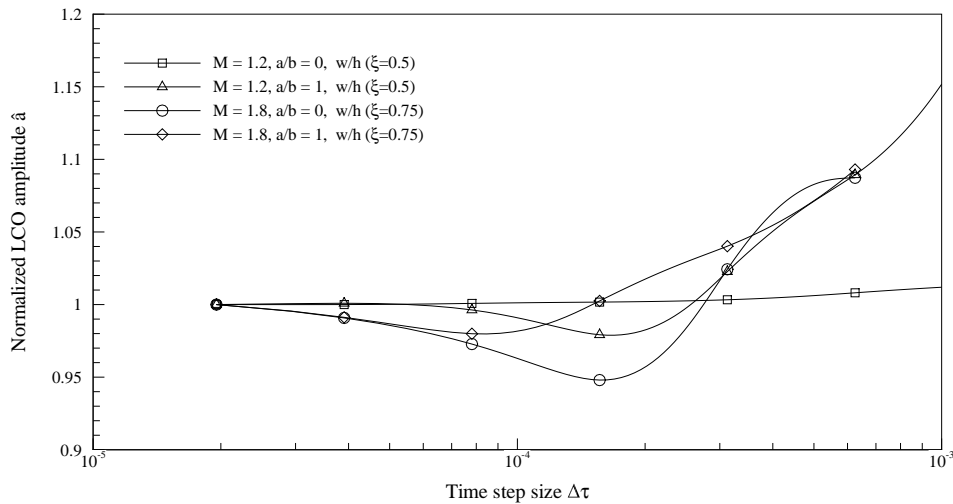
where  $r$  and  $p$  are the refinement ratio and the order of convergence. In this work the former is set to 2 and the latter to 1.75.  $F_s$  is the so called factor of satisfactory. Because this work focuses mainly on the investigation of the flutter boundaries a conservative factor of  $F_s = 3$  is chosen for the RTI of the flutter boundary computations. The calculated values are shown in table 5.1. In the following sections the solution is regarded as converged for a RTI value smaller than 3. Therefore  $d\tau$  is set to 0.001 for Mach numbers between 1 and 1.3. For higher values of  $M$  a time

**Table 5.1:** TRI values for the temporal resolution study of the flutter boundaries

$TRI_{d\tau}$	$M = 1.8$		$M = 1.2$	
	$\frac{a}{b} = 0$	$\frac{a}{b} = 1$	$\frac{a}{b} = 0$	$\frac{a}{b} = 1$
0.01 – 0.005, %	-	-	9.02	73.04
0.005 – 0.0025, %	48.45	53.55	4.73	16.93
0.0025 – 0.00125, %	19.14	24.41	2.97	8.30
0.00125 – 0.00063, %	7.68	9.95	1.11	3.53
0.00063 – 0.00031, %	3.38	4.66	0.74	2.11
0.00031 – 0.00016, %	1.83	1.18	0.18	1.74
0.00016 – 0.00008, %	0.81	0.89	0.14	0.50
0.00008 – 0.00004, %	0.66	0.65	0.11	0.29
0.00004 – 0.00002, %	0.01	0.22	0.02	0.04

step size of 0.0001 is applied.

Even if this work shall focus on determining whether a system is stable or not, some post flutter investigations were carried out to understand the character of the arising instabilities. Due to this another temporal resolution study was carried out to examine the influence on the amplitude of the flutter oscillations. Therefore the flutter solution for dynamical pressures 50% above the flutter boundary where computed for the same set of parameters as above. The obtained amplitudes are shown in Fig. 5.2 normalized to the amplitude of the finest time step size. The most

**Figure 5.2:** Results for the temporal resolution studies of the influence on the flutter amplitudes.

striking peculiarity on these results is that the curves start above the finest value and then cross the zero error line before they converge to the smallest chosen value. This indicates that for time step sizes above 0.0003 the oscillations computed by the software possess oversized amplitudes whereas calculations with lower values of  $d\tau$  yield to small amplitudes until converging for very fine time step sizes. Comparing the results to the temporal resolution study on the flutter boundaries the same behaviour for higher Mach numbers and length to width ratios can be observed. For the flutter amplitudes TRI values are calculated as well and presented in table 5.2. Because the post flutter behaviour is investigated rather qualitatively than quanti-

**Table 5.2:** TRI values for the temporal resolution study of the flutter amplitudes

$TRI_{d\tau}$	$M = 1.8$		$M = 1.2$	
	$\frac{a}{b} = 0$	$\frac{a}{b} = 1$	$\frac{a}{b} = 0$	$\frac{a}{b} = 0$
0.00125 – 0.00063, %	-	-	-2.28	-43.18
0.00063 – 0.00031, %	-8.75	-7.22	-2.07	-27.86
0.00031 – 0.00016, %	-11.45	-5.35	-0.67	-18.94
0.00016 – 0.00008, %	3.63	-3.28	-0.38	7.31
0.00008 – 0.00004, %	2.59	1.62	-0.21	1.99
0.00004 – 0.00002, %	1.30	1.25	-0.15	0.40

tatively the factor of satisfactory is set to  $F_s = 1$  and the RTI value representing a converged solution is set to 10. Hence a continuous time step size of  $d\tau = 0.0001$  was chosen for the post flutter computations.

## 5.2 Validation

For the purpose of validation the obtained stability boundaries are checked with the results from the literature. Therefore the automatically identified flutter boundary for a two-dimensional plate is compared with an application of the linearised potential flow theory carried out by Dowell[12] and with results from more recent investigations by Alder[21] based on Euler equations. Figure 5.3 shows the curves of all three computations. It can be seen that the solutions are generally conform. Comparing with the results of the earlier computation based on the linearized potential flow theory the whole Mach number range agrees to a great satisfaction. The obtained critical dynamic pressures for Mach numbers from 1 to 1.3 also conform exactly with the Euler equations. The results furthermore reveal that the present

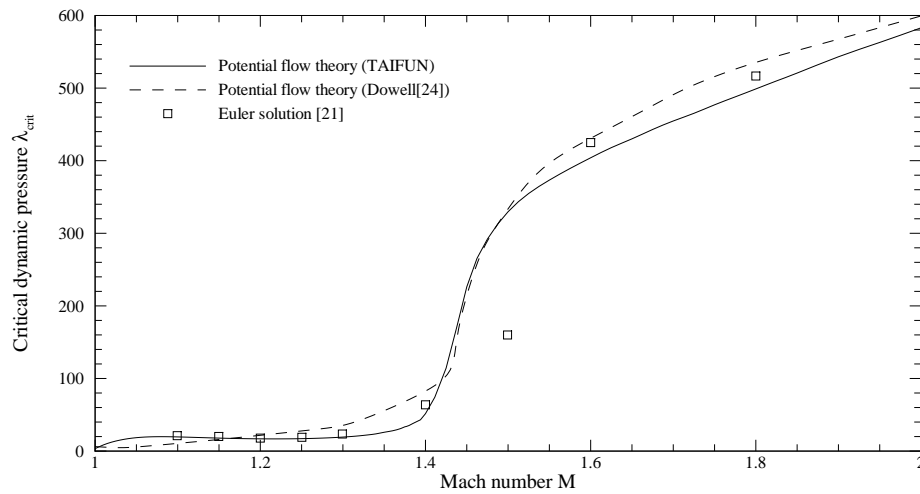


**Figure 5.3:** Stability boundary of a simply supported two-dimensional panel at low supersonic flow compared with results from Dowell[24] and Alder[21].

results better match the Euler computations compared to the results from Dowell. This may be explained by the limited computer capacity which was available for Dowell so that the stability curves are composed of fewer Mach numbers. It is furthermore difficult to extract the results for low Mach numbers from the associated publications. Also the higher region from  $M = 1.6$  to  $M = 2$  presents a good agreement. Only the Mach numbers from 1.4 to 1.6 show rather high deviations. As mentioned before, this region showed problems during the automatic analysis and thus the presented curve is fitted through the values calculated by the automatic identification. A detailed discussion of the complications in this region is given later in this chapter. To account for three-dimensional panel geometries the stability boundary of a squared panel is compared with the results from Dowell[12] in Fig. 5.4. Also the curves for the three-dimensional plate show good agreement to earlier flutter investigations based on the linearized potential flow theory. The critical dynamic pressures for the Mach numbers between 1.25 and 1.6 have been interpolated between the successfully computed values, too.



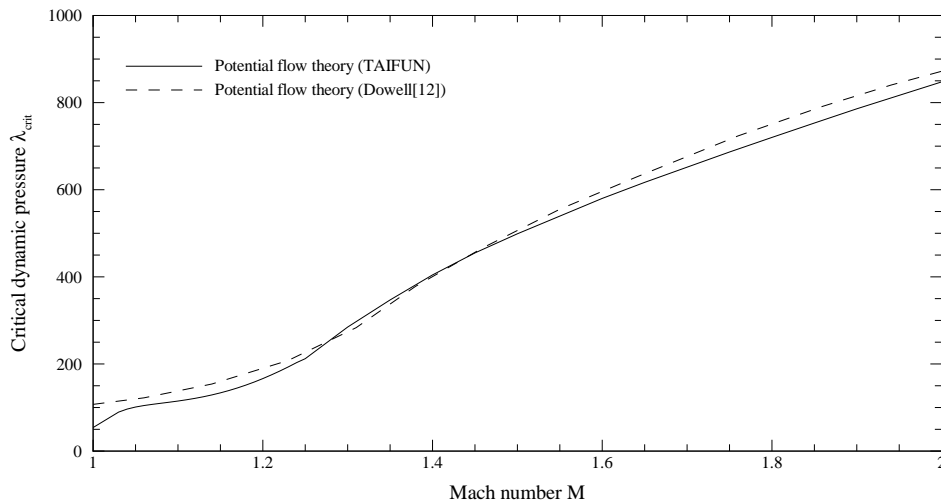


**Figure 5.4:** Stability boundary of a simply supported three-dimensional panel at low supersonic flow compared with results from the literature[12].

### 5.3 Results of the constant flow conditions

Several previous studies about panel flutter from the investigated literature stated the low supersonic Mach number region as an especially critical zone. Further it was shown in chapter 2.3 that the highest dynamic pressure acts in the very first seconds of the launch of a spacecraft. For these reasons the stability investigations of this region have been selected as the main focus within this work. Hence stability boundaries have been computed for several sets of parameter variations.

#### 5.3.1 Effects of the Mach number

##### Stability investigations

As shown in chapter 2.2.2 the Mach number has various effects on the stability as well as on the characteristics of an arising flutter motion. Caused by that, the first subject of investigation was aimed to yield flutter boundaries for the Mach number range from  $M = 1$  to  $M = 2$ . Because the investigated Mach number range is limited to these values, in the following values of the Mach number from 1 to approximately 1.4 are referenced as low supersonic and the range  $M = 1.6$  to  $M = 2$  as high supersonic. Values between these will be classified as moderate supersonic. In addition to the computations with a length to width ratio of 0 and 1, flutter boundaries

have been calculated for  $a/b = 0.5714$  and  $a/b = 1.75$ <sup>1</sup>. The four obtained stability boundaries are presented in Fig. 5.5. It can be seen that all curves show generally

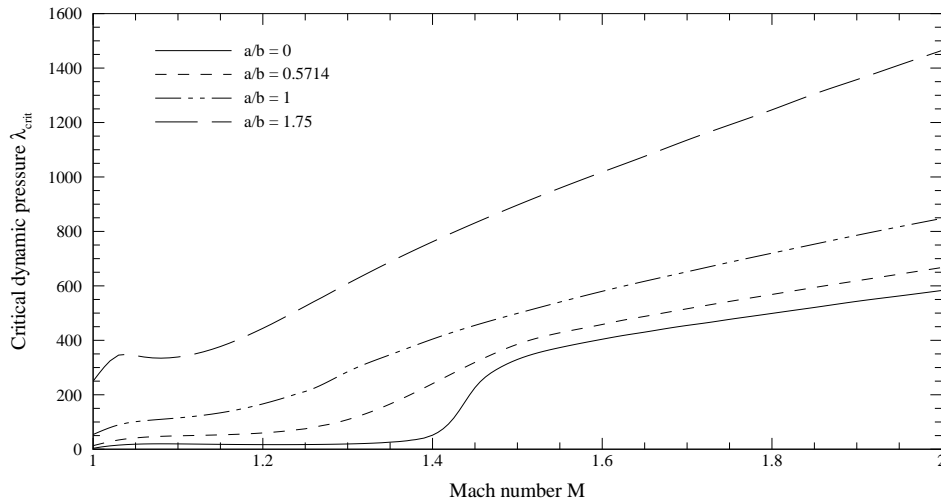


**Figure 5.5:** Stability boundaries of simply supported panels with different length-to-width ratios at low supersonic flow.

the same behaviour for a variation in Mach number. There exists a significant decrease of the critical dynamic pressure towards low supersonic Mach numbers. This is observed for all aspect ratios considered in the present work. If the Mach number is increased, the flutter boundary increases as well. However the curves increase in a different way. The two-dimensional panel experiences a decrease in critical dynamic pressure from  $M = 1.1$  to  $M = 1.3$  and then starts to climb slowly before it changes abruptly to a steep increase from a Mach number of 1.4 to 1.5. The range of high supersonic velocities then again exhibits a slight exponential growth. The curves for three dimensional panels all show a rather gentle change from the slow increase for low supersonic velocities to a steeper logarithmic increase for higher Mach numbers. Furthermore it can be seen that the turning point of these climb phases appears earlier with increasing length to width ratios.

### Modal participation

From the literature study it is known that the Mach number not only shifts the critical dynamic pressure but additionally affects the flutter mode shape. This means that a panel with a specific geometry exhibits a change in its flutter motion by pass-

<sup>1</sup>Values are chosen for future comparisons to wind tunnel tests at the German Aerospace Center.

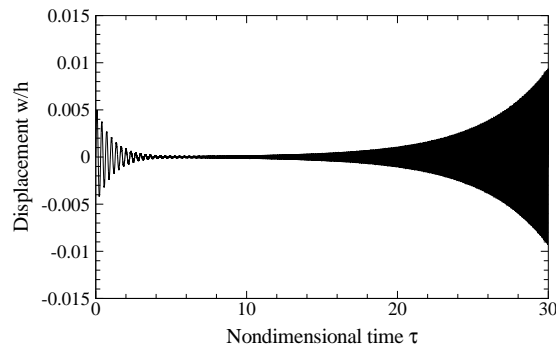


**Figure 5.6:** Establishment of a higher mode by an excitation of the first natural mode.

ing through different Mach number regions. Furthermore several previous chapters it already appeared that flutter oscillations in the vicinity of  $M = 1.4$  are significantly more complex and the automatic analyses failed. This is caused by contributions of the higher modes to the flutter motion which are excited very slowly, resulting in very large transients. Thus, the oscillations does not show a pure increasing or decaying pattern, but decreases first and then starts to grow again. This effect is shown in Fig. 5.6. Because in these regions the dominant acting mode changes rather abruptly the initial excitation would have to be adjusted for every iteration step. To apply the automatic iteration this would abolish its benefit. Further the oscillation itself is more complex and the identification of the maxima and minima is more complicated. Due to this observed complications the participation of the different modes and thus the shape of the panel deformations has been investigated in more depth. The results are shown in Fig. 5.7 to 5.11. The lower instability boundaries indicated by the dashed-dotted-lines in these illustrations have been obtained by using different modes as initial conditions. Because in reality not a specific mode is excited, identifying the stability boundary by using the finally arising mode appeared to be the more reasonable and, besides, the faster method. The figures 5.7 to 5.11 show the different flutter modes arising for the examined panel geometries. Figure 5.7 shows the critical dynamic pressures of a two-dimensional panel for a Mach number range from 1 to 1.8. The shape of the flutter boundary is already shown in figures 5.3 and 5.5. The curve is determined by an automatic identification of the solution type and a successive adjustment of the dynamic pressure as explained in section 4. The symbols illustrate the Mach numbers which have been computed by a manual adjustment of the dynamic pressure to verify the algorithm searching for the flutter boundary and to determine the shape of the flutter mode

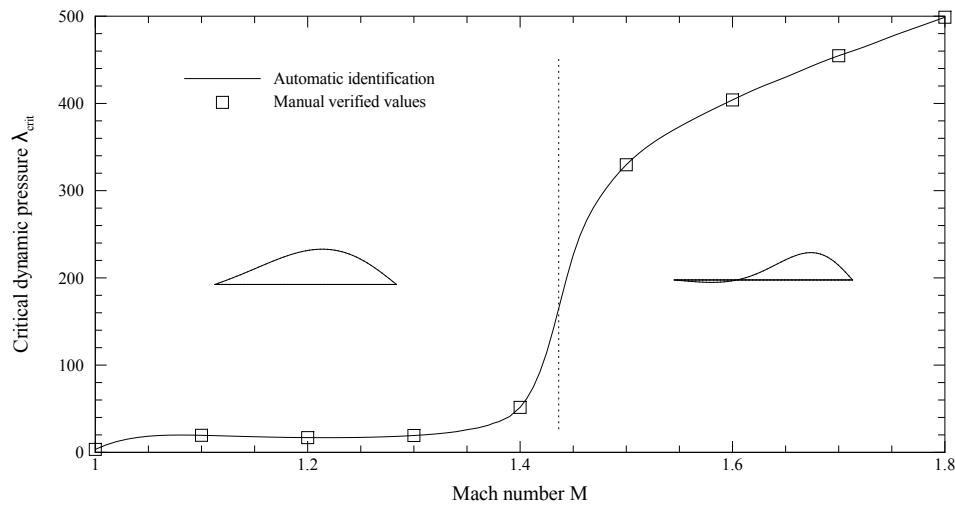


**Figure 5.7:** Stability boundary of a two-dimensional, simply supported panel with arising flutter mode shapes.

which arises for values slightly above the critical dynamic pressure. As can be seen for the values from  $M = 1$  to  $M = 1.4$  a shape very similar to the first natural mode of a plate was observed. For higher Mach numbers the shape changes to the one which is shown on the right hand side of the dotted line. These two modes look like a combination of mainly the first- and second natural modes as can be seen in Fig. 5.8. These two detected flutter shapes are typical shapes which are observed in comparable panel flutter studies in the literature. The first shape (I from B) has also been identified among others by Bendiksen and Davis[17] and the second (II from B) for example in Refs. [7] and [25].

In previous sections within this work it was already stated that because of interacting higher modes the program sometimes fails to identify whether an oscillation is damped or excited. These problems occurred for all three-dimensional plates ( $a/b = 0.5714, 1, 1.75$ ). Therefore it is no

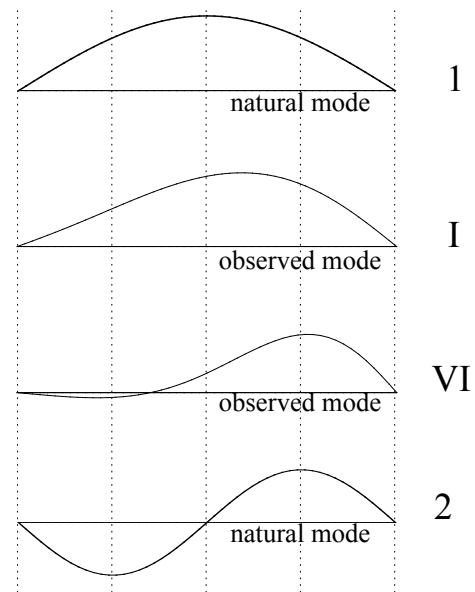


**Figure 5.8:** Observed mode shapes of the two-dimensional panel compared to the natural modes.

wonder that the arising mode shapes of these panels are more complex than for a two-dimensional plate. The observed mode shapes along the flutter boundaries of the panels with the length-to-width ratios  $a/b = 0.5714$ ,  $a/b = 1$  and  $a/b = 1.75$  from Fig. 5.5 are presented in Figs. 5.9 to 5.11. Within the illustrations the same stabil-

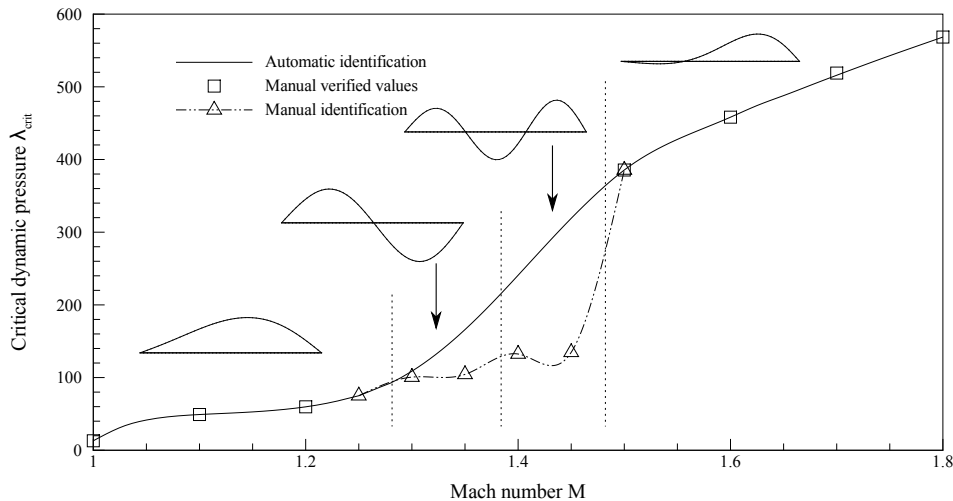


**Figure 5.9:** Stability boundary of a simply supported panel with  $a/b = 0.5714$  with arising flutter mode shapes.

ity boundaries as in Fig. 5.5 are presented, each in a distinct diagram. Furthermore as presented similarly in Fig. 5.7 the different arising flutter shapes are shown and the manual computed values again marked with a square symbol. As already stated each of these panels showed influences of higher modes for a specific range within the moderate Mach numbers. These regions not only showed more participating modes, but further yielded much smaller values of the critical dynamic pressures than the interpolated curves predict. These deviating values are indicated with little Deltas instead of the squares. Further a smaller stability boundary, obtained through the interpolation between the deviant values, is suggested by the dash-dotted line. For the panel with a length to width ratio of 0.5714 diverging critical dynamic pressure occurred between  $M = 1.3$  and  $M = 1.5$ . Within this range two more flutter shapes can be observed. For Mach numbers of 1.3 and 1.35 a shape similar to the second natural mode arises, whereas for  $M = 1.4$  to  $M = 1.5$  the shape looked like the third natural mode. The high supersonic velocities exhibits the same mode than for the two-dimensional panel. The squared plate exhibits even an enhanced range of deviating values. Manually obtained critical dynamic pressures started already for a Mach number of 1.25 to diverge from the estimated stability boundary and begin

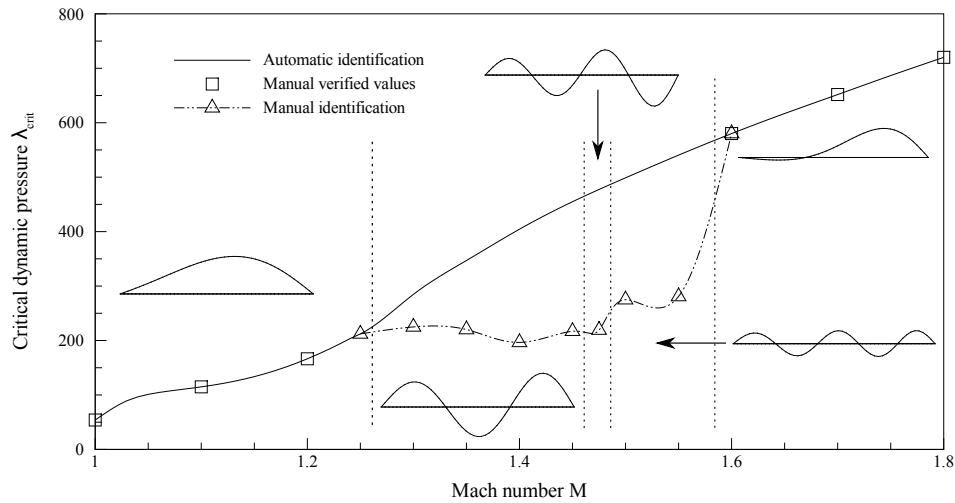


**Figure 5.10:** Stability boundary of a simply supported panel with  $a/b = 1$  with arising flutter mode shapes.

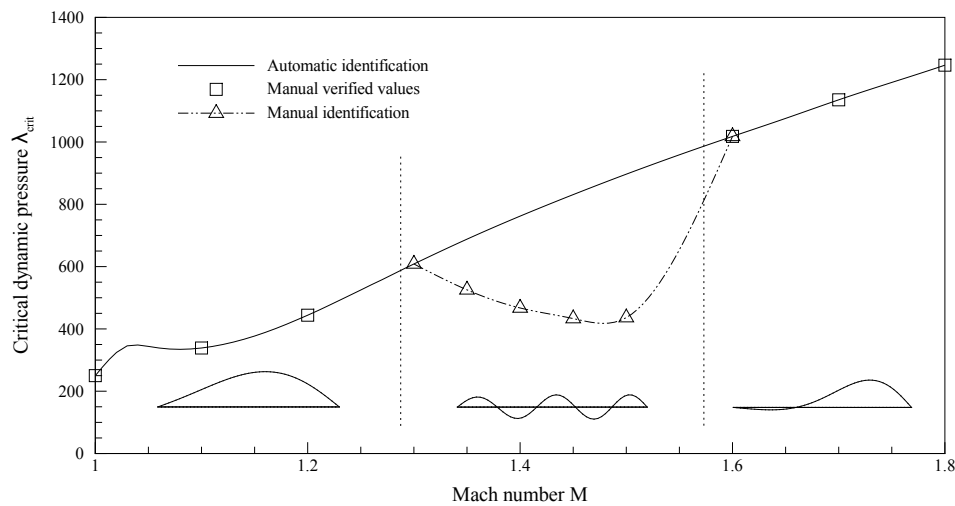


**Figure 5.11:** Stability boundary of a simply supported panel with  $a/b = 1.75$  with arising flutter mode shapes.

to agree with the automatic calculations for Mach numbers of  $M = 1.6$  and higher. Further the shape directly changes from the first mode alike to the one dominated by the third natural mode. This was observed until  $M = 1.4$ . For higher velocities also flutter shapes mainly influenced by the fourth or fifth mode arise for the LCO. Mach numbers from 1.6 onwards again show the well known mode obtained in many other investigations. For the computations of the panel with a length-to-width ratio of 1.75 only the fifth mode was observed within the range showing deviations from the approximated flutter boundary.

However, during the literature study flutter boundaries alike the ones indicated by the interpolated, dashed-dotted lines have not appeared in such manner in previous investigations. Therefore it cannot be excluded that these effects are caused by numerical inaccuracies. However the participation of higher modes in these regions has long been known and appeared repeatedly within the literature. Even more recent investigations as made by Davis and Bendiksen[31] who used Euler equations and a FEM method instead of the linearised potential flow theory in combination with the von-kármán plate theory, observed these effects. They showed that for Mach numbers as 1.4 and 1.5 higher modes establish according to Fig. 5.6.

### Post critical flutter behaviour

In order to get a insight and a better understanding in the complex effects of the previous stated regions, the flutter behaviour slightly above the critical dynamic pressure has been subject to brief investigations in this work. Thereby the arising amplitudes of the LCOs (caused by an increasing dynamic pressure) have been computed for three different Mach numbers, one from each velocity region (low-, moderate- and high supersonic). The results are presented for a length-to-width ratio of  $a/b = 0$  in Fig. 5.12 a and  $a/b = 1$  in Fig. 5.12 b. Amplitudes have been obtained for dynamic pressures of 100% to 200% of the flutter boundary. When comparing the three curves it is very obvious that the Mach number strongly affects the behavior of the flutter oscillation. Local amplitudes at a Mach number of 1.2 suddenly increase beyond the critical dynamic pressure, similar to a Hopf bifurcation. For the higher Mach numbers this growth becomes slower and the slope approaches a logarithmic growth. This indicates that the low supersonic region is not only more critical to the onset of flutter but further has to be considered more carefully for post-critical applications. Supplementary to the two-dimensional investigation LCO-amplitudes have been calculated for a square plate (5.12 b). The results of the three-dimensional computations show the same trend comparing  $M = 1.2$  and

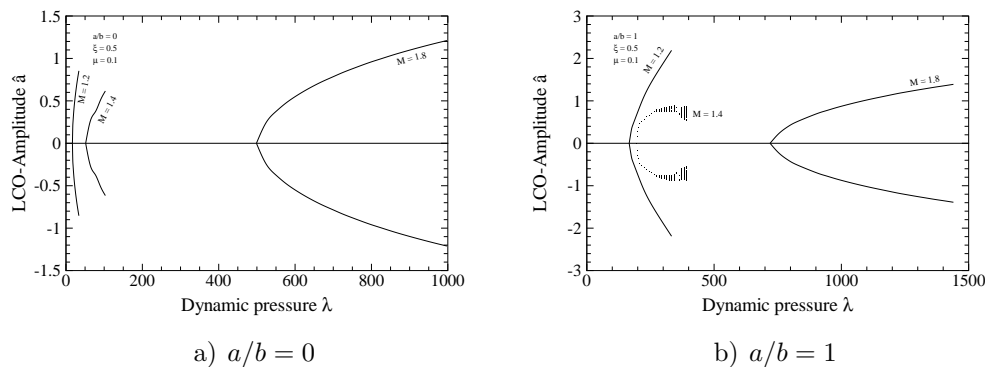


**Figure 5.12:** LCO-amplitudes for  $M = 1.2, 1.4, 1.8$  for simple supported panels with length-to-width ratios of 0 (a) and 1 (b).

$M = 1.8$ . The curve of the Mach number of 1.4 shows a more complex behaviour. This behaviour is conform with the previous identified participation of higher modes in the moderate supersonic velocity region. The curve representing this range shows the same behaviour until a dynamic pressure of 140% of the flutter boundary is reached. For higher values of  $\lambda$  different oscillations interfere with each other and various periodic extrema occur presented by points instead of a continuous line. This outcome shows that the previous identified influences of the higher modes for Mach numbers about 1.4 also appear in the post critical regions. Except for these effects the observed general tendency is conform with the results of ref. [22] presented in chapter 2.2.2. Due to the focus on the stability investigations of this work a deeper investigation of the effects of the chaotic behaviour is omitted, while the reader is referred to Refs. [32], [33] and [34].

### 5.3.2 Effects of the length-to-width ratio

#### Stability investigations

In the literature study it already appeared that the length-to-width ratio has a stabilising effect on panel flutter. This influence is illustrated by Fig. 5.13. Herein three different curves are shown, each representing a specific Mach number. The general influence of the length-to-width ratio is the same for every Mach number. It can be seen that the critical dynamic pressure shows an exponential growth for an increase of  $a/b$ . Further the influence of the Mach number, already known from the previous chapter, can be seen. An increase leads to an upwards shift of the curve.



The slopes of the curves for the low- and high supersonic mach numbers are very similar. The only difference is that the Mach number of 2 shows a faster growing increase.

The instability boundary of  $M = 1.414$  again exhibits a special behavior. The crit-

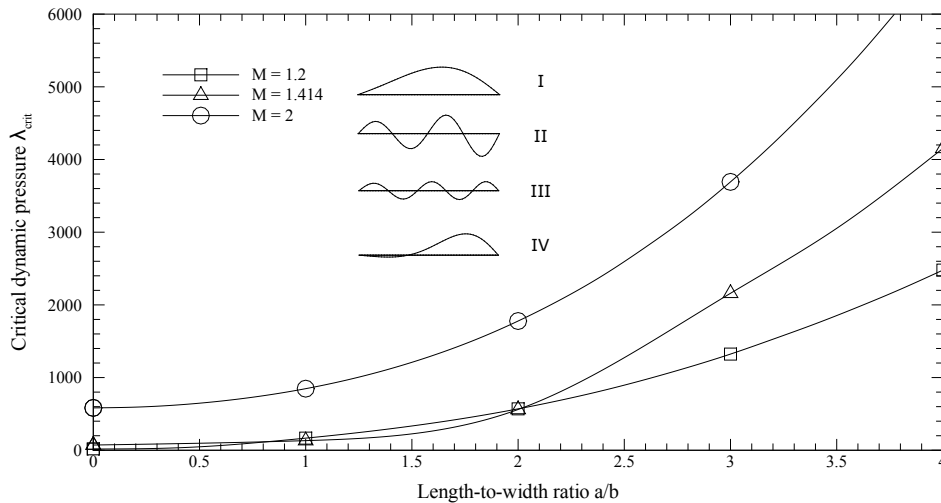


**Figure 5.13:** Stability boundaries in dependency of the length-to-width ratio for different Mach numbers.

ical dynamic pressure is, accordingly to the general trend, higher than for a Mach number of 1.2. If the length-to-width ratio is increased, the two curves intersect and the flutter boundary of  $M = 1.414$  becomes lower than for the smaller Mach number. This behavior changes again after another intersection at  $a/b = 2$ . From this value onwards the higher Mach number yields higher values for the critical pressure and the curve shows an exponential growth for an increase in length-to-width ratio. This effect is only observed for the moderate range of supersonic Mach numbers and is again caused by the participation of the higher modes. Comparing figures 5.7 to 5.11 the same effect can be observed. For some Mach numbers the critical dynamic pressure of the three-dimensional panels drops below the values of the one-dimensional plate. The influence of other modes can also be seen by examining the flutter mode shapes. This is done for selected  $a/b$  values of the curve which represents  $M = 1.414$ . The arising LCO shapes are indicated by the roman numbers in fig. 5.13. For a length-to-width ratio of 1 the main acting mode is the third natural mode. For  $a/b = 2$  the flutter shape is very similar to the fifth natural mode of a plate. For higher length-to-width ratios the typical shape of the high supersonic region establishes and the slope of the curve changes to an exponential

increase according to the general trend. This suggests that the higher modes only participate in specific ranges of  $a/b$  and  $M$ .

### Post-critical flutter behaviour

Similar to the Mach number effects, the influence of the length-to-width ratio on the post flutter behavior has been subject of some further investigations. As already stated in the literature study in chapter 2.2.3 a change in  $a/b$  creates a much weaker influence on the solution than a variation of the Mach number. This can be seen in figure 5.14. Herein the local LCO-amplitudes of panels with different length-to-

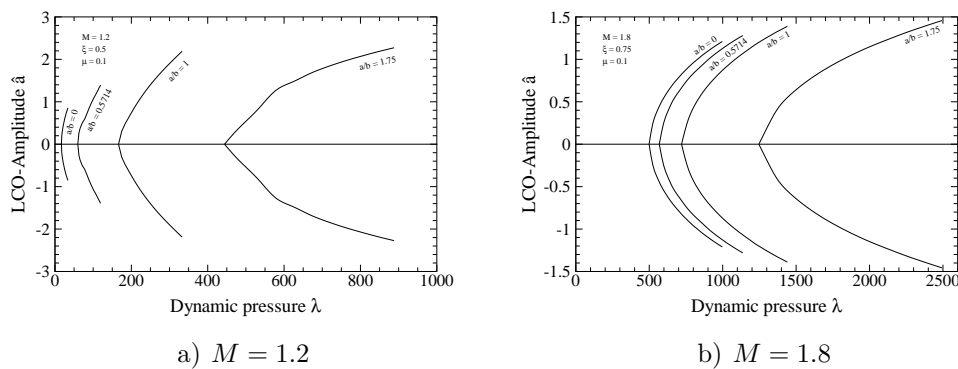


**Figure 5.14:** LCO-amplitudes for  $a/b = 0, 0.5714, 1, 1.75$  of simple supported panels at (a) low- and (b) high supersonic velocities for dyn. pressures until  $q/q_{crit} = 2$ .

width ratios are presented. The picture on the left hand side shows the amplitudes obtained with a Mach number of 1.2, the one on the right hand side represents the high supersonic velocities at  $M = 1.8$ . Comparing these curves, it can be seen that the higher values of  $a/b$  yield curves with smaller slopes. This means that panels with larger length-to-width ratios exhibit a slower growth of their LCO-amplitude if the dynamical pressure is increased. Nevertheless, compared to the influence of the Mach number, the qualitative differences of the curves are very small. The same observations can be made by comparing the amplitudes of the same panel geometries in a supersonic flow at  $M = 1.8$ . This is shown in figure 5.14 b. The obtained results represent that the length-to-width ratio heavily influences the local LCO-amplitude but has no effect on the qualitative shape of the curves. In fact the dynamic instability sets in at higher dynamical pressures for larger values of  $a/b$ , which corresponds to the influence of the ratio of the panel length and width on the

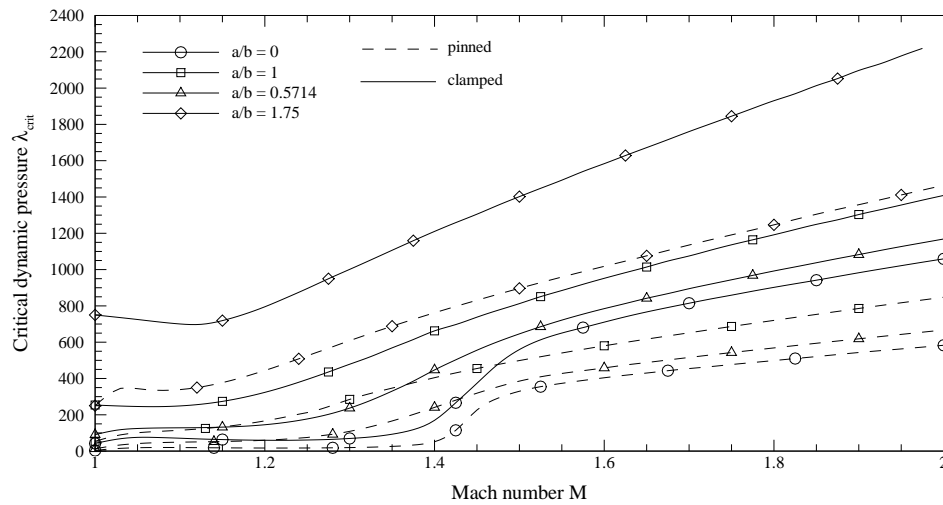


**Figure 5.15:** Comparison of stability boundaries for clamped and pinned panels with different length-to-width ratios.

critical dynamic pressure. Although the curves are merely shifted towards larger dynamic pressures, they but possess a comparable slope.

### 5.3.3 Effects of the boundary conditions

To compare flutter phenomena of pinned and clamped panels, similar stability investigations to the ones carried out for the pinned panels described in chapter 5.3.1 and 5.3.2 have been conducted with equivalent clamped plates. The outcome is presented and opposed with the results of the pinned panels in figure 5.15. A general trend is obvious. The clamped panels yield flutter boundaries which show a good qualitative agreement to their pinned counterparts. However, the main influence of the clamped boundary conditions is that it shifts the stability boundary upwards. Hence, the dynamic pressure at which flutter arises for a clamped panel is larger than for an identical pinned panel. Regarding the curve of the panel with a length-to-width ratio of 0.5714 it can be seen that changing the boundary conditions from simply supported to a clamped panel raises the critical dynamic pressure above the one of a pinned square panel.

Comparing the flutter boundaries over a range of several length-to-width ratios for pinned and clamped plates a very similar influence can be observed. This is illustrated in figure 5.16. The curves of the flutter boundaries obtained by the compu-

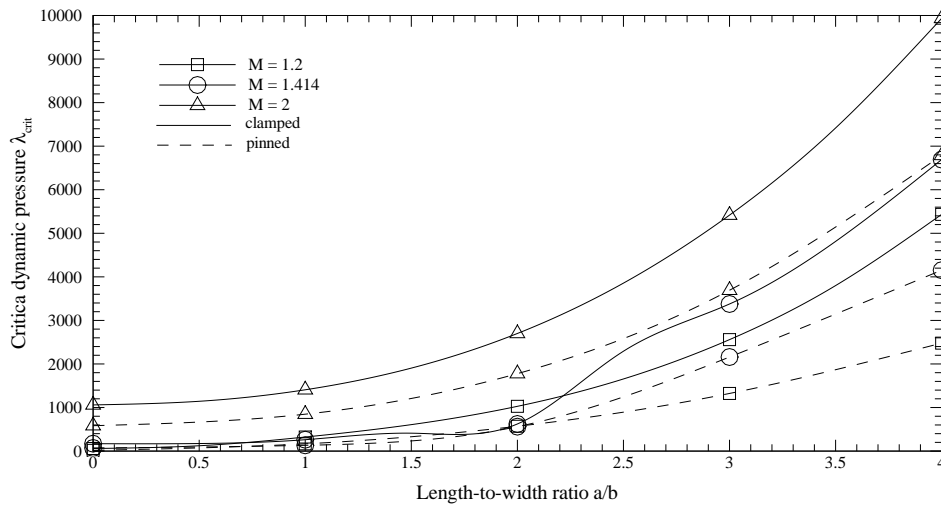


**Figure 5.16:** Comparison of stability boundaries over a range of different values of  $a/b$  for clamped and pinned panels at different Mach numbers.

tations with clamped boundary conditions are shifted upwards in an equal manner as discussed in the framework of a variation of the Mach number. The slopes of the curves are again scarcely influenced. Here the instability boundary at a Mach number of 1.414 as well intersects with the curve representing  $M = 1.2$  and possesses lower critical dynamic pressures over a range of  $a/b = 0.75$  to  $a/b = 2.25$ . This shows that the clamped panels exhibit the same interferences of the higher mode as it has been observed with simply supported boundary conditions. This results have been verified by manual identifications of the flutter boundary and the oscillation shapes, respectively to the computation of the pinned plates. Because displaying similar curves to the ones shown in figures 5.7 to 5.11 would not yield further insights such illustrations are omitted. However, in table 5.3 the dominant modes observed in these investigations are presented and compared with the mode shapes which have been discovered for simply supported panels. For an explanation of the given mode shape numbers refer to appendix B. The observed mode shapes represent mainly coincidence. Given identical conditions ( $M$  and  $a/b$ ) generally the same dominant modes arise for pinned and clamped plates. For some Mach numbers the clamped panels already change to the next higher mode whereas pinned boundary conditions do not change until higher Mach numbers. Furthermore for the clamped panels the interference of higher natural modes is observed up to higher Mach numbers. The computations with clamped edges show such influences up to

**Table 5.3:** Dominant mode shapes for pinned and clamped panels in the Mach number range from 1.2 to 1.8.

$M$	$a/b = 0.5714$		$a/b = 1$		$a/b = 1.75$	
	pinned	clamped	pinned	clamped	pinned	clamped
1.2	I	I	I	I	I	I
1.3	II	III	III	III	V	V
1.4	III	III	III	III	V	V
1.5	VI	III	V	III	V	V
1.6	VI	V	VI	V	VI	V
1.7	VI	VI	VI	VI	VI	V
1.8	VI	VI	VI	VI	VI	VI

Mach numbers of 1.6 and 1.7. The pinned panels yielded the typical shape (VI) for these Mach numbers.

## 5.4 Results of the time variable flow conditions

In the following sections several computations are presented using the program feature which allows to vary the Mach number and the dynamic pressure with time. Because no similar investigations were conducted in the literature a validation by comparison is not possible. However the results are analysed and checked for agreement with the expectations which arise from the physical foundations. Therefore trajectories derived from the Saturn V rocket are used within the computations. The process of deriving these trajectories is described in the first subsection. In the following parts the different computations are presented.

### 5.4.1 Trajectory computations

The purpose of the temporal adjusting integration is to study the influence of changing flow conditions during flutter. Therefore the trajectories which are used as input source for the Mach number and the dynamic pressure are derived from the Saturn V trajectory presented in chapter 2.3. The values taken from Ref. [28] are converted into a non-dimensional notation. This yields a trajectory defined by three parameters: the non-dimensional time  $\tau$ , the Mach number  $M$  and the non-dimensional dynamic pressure  $\lambda$ . To identify the trajectories which are interesting for the sake of

stability investigations, it is fertile to express the dynamic pressure in dependence of the Mach number. This enables an easy examination of the dynamic pressure for each Mach number. Regarding the equation to convert the dynamic pressure into the non-dimensional dynamic pressure

$$\lambda = \frac{\kappa M^2 a^3}{D} p_\infty \quad (5.2)$$

the isentropic exponent is set to constant. The pressure is dependent on the density of the flow and thus corresponds to the actual altitude. The trajectory can be shifted upwards or downwards by changing the structural ratio  $a^3/D$  defined by the length of the panel  $a$  and the stiffness  $D$ . Hence by adjusting this ratio, the dynamic pressures can be changed and the trajectory is shifted but still retains the qualitative relation of the dynamic pressure and the Mach number from the Saturn V trajectory. This method is used in this work to obtain the trajectories which shall be investigated. It is important to note that by changing  $a$  and  $D$  not only the dynamic pressure, but also the non-dimensional time  $\tau$  changes due to the conversion by

$$\tau = t \cdot \sqrt{\frac{D}{\rho_m h a^4}} \quad (5.3)$$

The chosen trajectories are presented in Fig. 5.17 and are numbered for the sake of referencing with capital letters (referring to the type of trajectory) and numbers (representing the length-to-width ratio). It can be seen that all trajectories cross

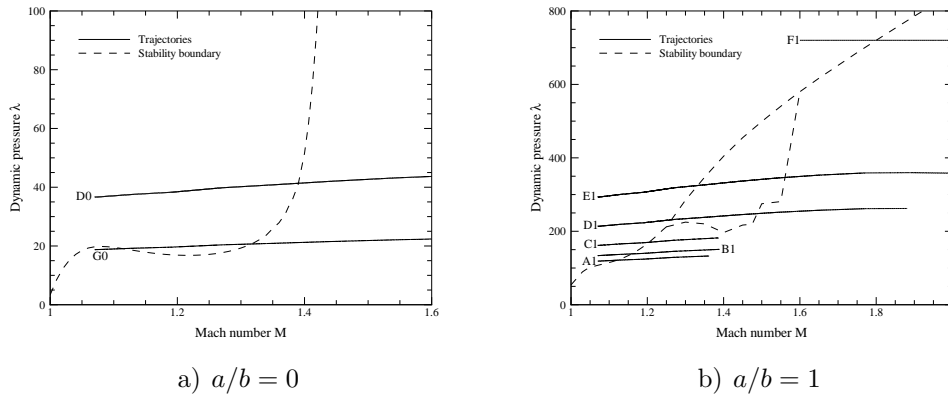


**Figure 5.17:** Illustration of the computed trajectories shifted by a change in the structural parameter  $a^3/D$ .

the stability boundary. This was picked as the most interesting behavior because it

represents a spacecraft which is exposed to stable as well as unstable regimes during its flight. Because of that the points of interest chosen by the author are trajectories which reproduce such situations. Therefore computations are carried out simulating a start in the unstable region and then crossing the stability boundary and entering the stable region. As it can be seen this setting is examined for several different magnitudes of the dynamic pressure. Figure 5.17 only presents the trajectories of the panels with length-to-width ratios of 0 and 1. The two other panels are omitted because the main fraction of investigations is carried out for the squared panel. Nevertheless selected trajectories (D and F) are computed for each panel geometry, though these are similar to the corresponding trajectories for  $a/b = 0$  and  $a/b = 1$ . For the one-dimensional panel it is even possible to start the trajectory within the stable region, cross the unstable region and finally reenter the stable area again. The precise reasons for each trajectory will be explained alongside with the outcome of the computations in the following sections.

#### 5.4.2 Trajectories traversing the stability boundary

The first question which arises when regarding the trajectories and the stability boundary in figure 5.17 is how a panel behaves if it crosses the flutter boundary from the unstable to the stable region. To obtain an answer computations are carried out simulating such a situation for the different panel geometries (D of Fig. 5.17). The resulting deformations for length-to-width ratios of 0 and 1.75 are presented in figures 5.18 and 5.19 over the range of crossed Mach numbers. This is done to facilitate a direct comparison of the actual dynamic pressure, which the panel exhibits at a specific Mach number and the critical dynamic pressure. Thus, the actual deflection at a specific Mach number can be attributed to the relation of these pressures. The values of the dynamic pressures  $\lambda_{act}$  and  $\lambda_{crit}^*$  are presented on the right hand side of the figures. The displacements are shown on the left hand side. Regarding the figure illustrating the computation of the one-dimensional plate it can be seen that the deflection of the panel (shown by the dotted line) growth very rapidly in the beginning and then begins at a Mach number of approximately  $M = 1.2$  to decrease until the solution almost damps out completely towards  $M = 1.7$ . This behavior is very conform with what is expected. It is straight forward that the deformations increase within the unstable region and, after crossing the stability boundary, drop to zero. However, the intersection of the actual dynamic pressure (solid line) with

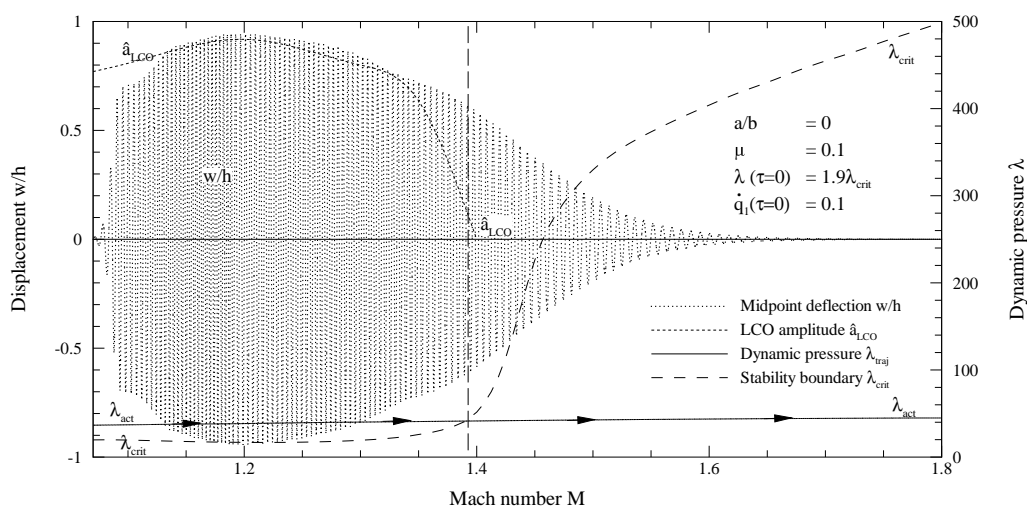


**Figure 5.18:** Computation of a trajectory crossing the stability line for a two-dimensional panel.

the flutter boundary occurs at a Mach number slightly below 1.4 instead of 1.2. This indicates that the motion of the panel begins to abate quite a while before dropping below the critical pressure  $\lambda_{crit}^*$ . Because of that steady computations have been carried out for fixed points from the trajectory. The amplitudes of the LCO  $\hat{a}$ , which arise under circumstances of infinite time are presented by the small dashed line. In the following the terms LCO and steady computations both reference the values obtained by these computations for an infinite time span. Comparing these with the actual deflection of the trajectory it can be seen that the motion of the plate follows the LCO amplitude generally very well and that the pre-critical decrease is caused by a drop of the LCO amplitude. The stationary amplitude of the Mach number range of about 1.1 is reached very fast after the excitation. Then the maximum deflections adapt to the LCO amplitudes until approximately,  $M = 1.35$ . After this value a rapid drop in the arising amplitude of the LCO can be observed. The deflections of the panel traversing the trajectory however drop much slower with a significant 'delay'. This is a very interesting phenomenon and is probably caused by the memory of the fluid defined by the admittance functions. This suggests that the past deformations and velocities of the panel influence the adaptation to the steady state. Furthermore the aerodynamic damping approaches zero towards the stability boundary. Hence, the motion of the panel settles very slowly.

Regarding Fig. 5.19 which shows a similar trajectory for the panel with the length-to-width ratio of 1.75 a related behavior can be observed. The panel motion as well



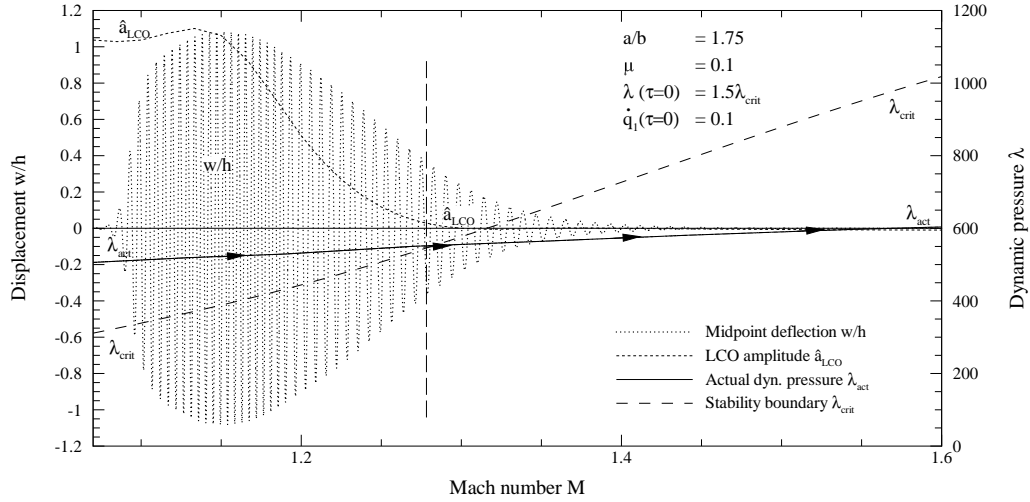


**Figure 5.19:** Computation of a trajectory crossing the stability line for a panel with a length-to-width ratio of 1.75.

shows a rapid increase until the magnitude of the LCO amplitude is reached. After the amplitudes of the stationary computations begin to decrease. The deflections of the panel traversing the trajectory follow again in a delayed fashion and hence still possess considerable dimensions when the actual dynamic pressure drops below the critical pressure. Thus both trajectories shown here possess generally the same characteristics. Both calculations yield a delay with respect to the steady computations. Comparing the fade away periods, the two-dimensional panel is decayed completely after traveling through a Mach number range with a span greater than  $\Delta M = 0.3$ . The panel with a length-to-width ratio of 1.75 is completely faded away at a Mach number approximately 0.175 larger than the one at which the stability boundary is crossed. Regarding the trajectories the non-dimensional time span to fade away is of a magnitude of 21.12 for the one-dimensional computation, whereas the panel with  $a/b = 1.75$  takes only  $\Delta\tau = 2.25$  to die out completely. Considering all factors but this structural parameter as constant, the actual (dimensional) time which is taken to travel along the trajectory has to be equal. The different non-dimensional time spans arise only during the conversion into non-dimensional units by making use of equation 5.3 due to the different values of  $D/a$ . A further distinction of both trajectories which is a possible reason for differences in the delay is the initial dynamic pressure. The two-dimensional panel starts with a magnitude of 1.9 times the critical dynamic pressure whereas the panel with  $a/b = 1.75$  only exhibits a magnitude of  $\lambda(\tau = 0) = 1.5\lambda_{crit}^*$ . This should mainly influence the initial growth,

but could also be a cause for different delays. To evaluate the individual influence of all mentioned conditions further investigations focusing each on one parameter are presented in the following chapters.

### 5.4.3 Trajectories traversing the transonic dip

In chapter 5.4.1 it was already observed that for a one-dimensional case a trajectory which crosses the transonic dip (G0 from Fig. 5.17) can be computed. Thus, the panel would cross the stability boundary in several instances. Such a trajectory is shown in Fig. 5.20, which starts in the stable region and then crosses the stability boundary accessing the unstable region before finally entering the stable area again. Regarding the shown displacements, the outcome is again very conform with rational

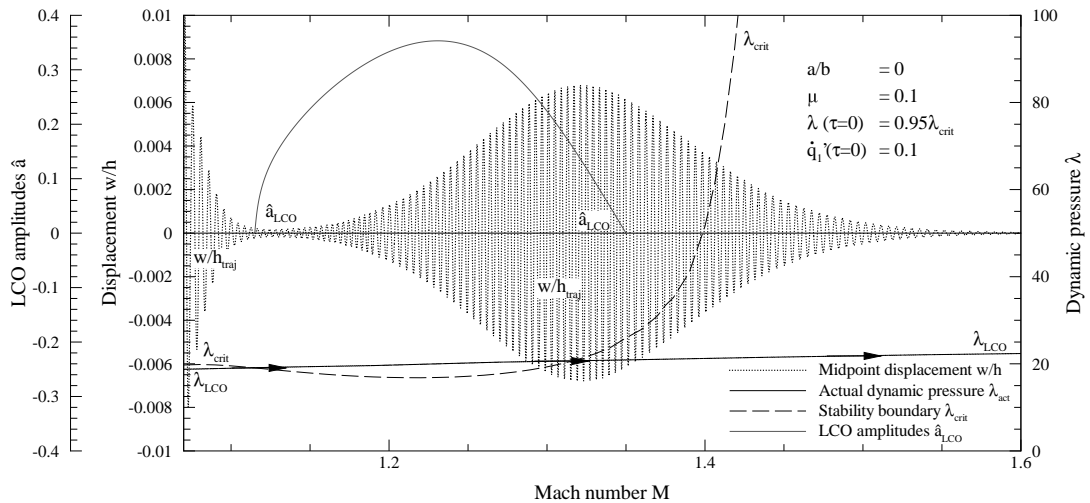


**Figure 5.20:** Displacements of a two-dimensional panel with a trajectory traversing through the transonic dip.

expectations. The initial excitation decays while the panel resides in the stable region. After crossing the flutter boundary for the first time at approximately  $M = 1.115$ , the panel displacements begin to increase until the reentry into the stable region at a Mach number of 1.315. From this point onwards the deformations slowly decrease until zero. This is a very reasonable behavior. However, comparing the actual deformations of the panel to the arising amplitudes of the LCO, a rigorous deviation can be observed. Herein the amplitudes of the steady computations are presented on a separate axis due to the large difference. Comparing the maximum

values of both, it can be seen that the actual deformations only reach a magnitude which equals two percentage of the maximum amplitude attained by the steady computations. This is a very dramatic difference and suggests that a spacecraft flying along such a trajectory would only exhibit a very small fraction of the load which would arise for infinite long computations. A very plausible reason for this result is that for states close to the stability boundary the damping or excitation is very small. Hence, the arising LCO takes a long times to settle. Furthermore, it has appeared in the investigations presented in the previous chapters that some mode shapes arise very slowly. For a spacecraft traversing this regions very rapidly the oscillation is not given enough time to raise to high magnitudes before the panel is already exposed to different conditions. This is a very important outcome for the sake of the structural dimension of such vehicles.

#### 5.4.4 Influence of the difference in the dynamic pressure

In chapter 5.4.3 it is observed that the displacements of the panel do not reach significant magnitudes compared to the amplitudes of the LCO. The most forward reason for this is stated as the small distance from the critical dynamic pressures. To investigate this, computations have been carried out for trajectories with different distances above the stability boundary for a squared panel (A1, B1 and C1 of Fig. 5.17). These distances in the dynamic pressure (and the following mentioned distances) all reference to the critical pressure at the Mach number of the first point of the trajectory. Three of these are presented in Fig. 5.21. Regarding the first

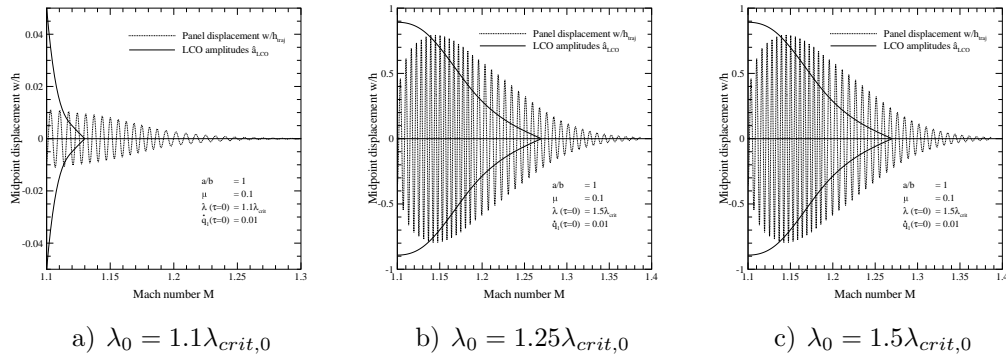


**Figure 5.21:** Trajecotries with different distances from the stability boundary.

illustration, which has been obtained for a start at only 10% above the critical dy-

dynamic pressure, it can be seen that the displacement of the panel only reaches a small fraction of the magnitude of the LCO amplitudes. Comparing again the maximum values, only 16.6% of the magnitude of the steady computations is obtained. Due to the small distance the panel enters the stable region almost directly after the start. Further the magnitude of the deflections of the LCO is very small. All these circumstances can contribute to only attaining a small fraction of the steady results. However, a similar outcome can be observed for the second case which represents a distance above the stability boundary of 25% in the dynamic pressure. Still only around 35% of the LCO-amplitude is reached even if the time until crossing the stability boundary is nearly doubled and hence the steady computations yield significant panel deformations. Comparing the previous described computation with the third shown trajectory (5.21 c), much higher panel displacements can be observed. For a start at a dynamic pressure of 50% above the critical value the deformations reach approximately equal magnitudes to the amplitudes of the LCOs. Summarizing the outcomes of the three computations it can be concluded that the size of the deflections increases very fast with a growing distance above the stability boundary. However, even if the trajectory with a difference of 10% above the critical pressure corresponds to the trajectory traversing the transonic dip, the latter reaches a much smaller fraction of the steady results. This is probably caused by the circumstance that the initial excitement is already damped due to the start in the stable region. Therefore the actual displacement when entering the unstable area is drastically reduced. However due to the phase within the region above the flutter boundary the panel already possesses past deformations and velocities. These support the increase of the displacement which can be observed in Fig. 5.20 after the stability boundary is crossed. However, despite the effect created by the memory of the fluid only small magnitudes are obtained. Regarding again Fig. 5.21 despite the differences in the magnitude of the displacements all three computations show the same delay which has been observed at the computations presented in chapter 5.4.2. This shows that such a behavior is obtained irrespectively of the 'path' of the trajectory.

### 5.4.5 Influence of the initial excitation

From the outcome of the previous chapters it is known that the flutter displacements are heavily reduced by approaching towards the instability boundary. However, it is obvious to assume that the reached magnitudes of the deformations depend on

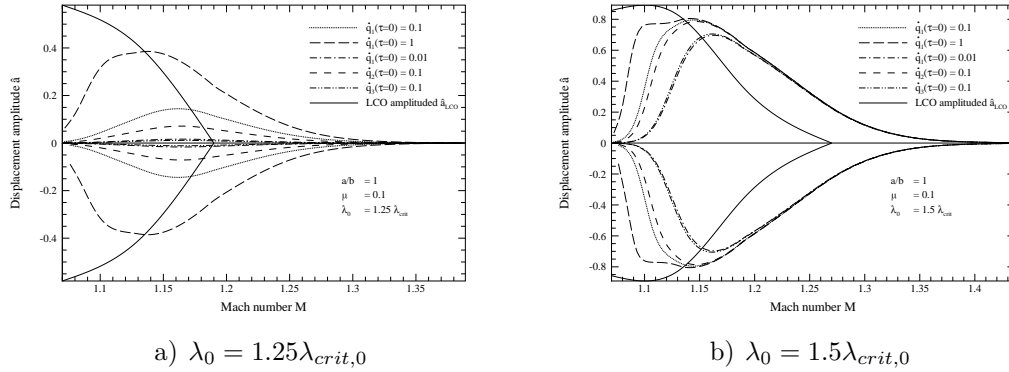


**Figure 5.22:** Computed trajectories with a distance of 25% and 50% above the dynamical pressure with a variation in the initial excitation.

the initial excitation. The previous presented investigations are all excited with an initial velocity of the first natural mode of the magnitude of 0.01. To examine the influence of the initial conditions the trajectories B1 and C1 are computed with different magnitudes of the excitation ( $\dot{q}_1 = 1, 0.1, 0.01$ ) and further computations with an excitation of the second and third mode ( $\dot{q}_2 = 0.1, \dot{q}_3 = 0.1$ ) are executed and presented in Fig. 5.22. The outcomes confirm the influence of the initial conditions. Especially for the trajectory closer to the flutter boundary (Fig. 5.22 a) the reached amplitudes grow drastically with the magnitude of the excitation. The computation with the initial condition of  $\dot{q}_1 = 1$  even reaches displacements comparable to the LCO amplitudes of the steady computations. The panel excited with a magnitude of 0.01 in the velocity of the first mode only exhibits deformations smaller than 0.05. Comparing the excitation in the velocity of the different natural modes it can be seen that the deformations induced by the excitation of the second and third mode are significantly smaller than for the first mode. This is assumed to be caused because the dominant mode for the computations is the first mode and thus this mode has to establish first before the amplitudes can rise to larger magnitudes. This explanation is supported by the fact that the motion following from the excitation of the third mode is smaller than for the second. The second mode changes faster to the first mode than the third mode does. Therefore the oscillation can grow to larger amplitudes. For all used initial conditions the dominant acting mode is the first and the mode shape III (refer to appendix B) was observed. The outcome of the trajectories starting at 50% above the critical dynamic pressure shows good agreements. The smaller the magnitude of the excitation the smaller are the reached

amplitudes of the deformations. However, the differences in the displacements are much smaller than for the trajectory starting at 25% above the stability boundary. As discussed in the previous chapter the damping and excitation of the oscillation is larger for higher differences to the critical dynamic pressure and thus even small excitations can reach large amplitudes in a shorter while. Similar to the computations starting at 25% above the critical dynamic pressure the magnitude of the displacements decrease with higher numbers of the excited natural modes.

### 5.4.6 Influence of the travel time

To examine the delay in more depth this subsection focuses on the individual influence of the time needed to travel through the Mach number regions. This non-dimensional time-span is defined as

$$T = \tau_{end} - \tau_{start} \quad (5.4)$$

and in the following will be called 'travel time'. Investigations have been carried out in which  $T$  is varied and all further elements are considered constant( Fig. 5.23). Herein deformations of a panel flying along a trajectory according to the Saturn V,

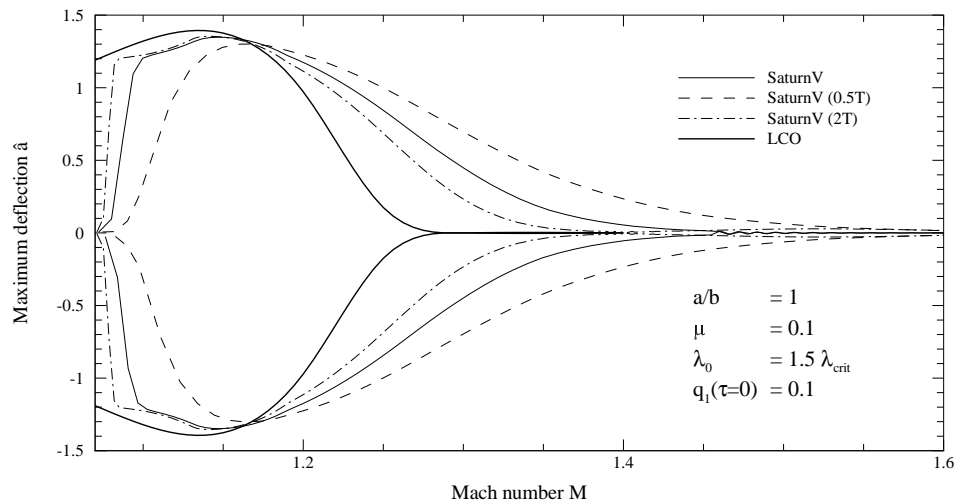


**Figure 5.23:** Saturn V trajectory fitted for  $a/b = 1$  crossing the flutter boundary with different travel times.

fitted for the panel with  $a/b = 1$ , are shown as well as the same trajectory with

double and half travel time  $\Delta\tau$ . For the sake of an easy comparability only the amplitudes  $\hat{a}$  are presented. The resulting curves very well demonstrate that the travel time heavily influences the magnitude of the delay. Comparing each curve with the amplitudes of the LCOs it is obvious that the smaller the travel time the closer the amplitudes converge to the steady computations. This applies for the decay phase as well as for the growth directly after the excitement. Even for the shortest travel time this initial growth is fast enough to reach the highest magnitude of the LCO amplitudes. This shows that even if the velocity of the spacecraft is increased in a very fast way, the panel deflections are likely to assume large proportions. A possible cause for this behavior is again the memory of the fluid which encourages the initial growth but retards the decrease of the amplitudes. This investigations confirm that the travel time influences the delay in the manner that an increase in  $T$  leads to a adaption to the LCO within a smaller Mach number range. Regarding the first introduced trajectories (Figs. 5.18 and 5.19) again the fact, that the three-dimensional panel shows a less distinct delay despite the influence of the travel time, may arise due to the geometry differences or caused by the fast drop of the LCO amplitude of the two-dimensional panel.

#### 5.4.7 Influence of the panel geometry

Further trajectories have been computed with a fixed time-span and identical initial conditions in the manner that the computation is started for a point with qualitatively the same differences in the dynamic pressure and Mach number from the critical values. Regarding the shown trajectories of the different panels (Figs. 5.7 5.11) all four curves possess an approximately similar slope for the Mach number range from 1.6 to 2. Because of that, this region has been selected with the aim to facilitate an preferably identical starting point for all panel geometries. Therefore all trajectories are defined to cross the stability boundary at a Mach number of 1.8 starting at  $M = 1.6$ . Regarding equation 5.3 and because of the equal travel time  $T$ , for all computations the plate length  $a$  and stiffness  $D$  have to be considered as constant to enable an identical dimensional time  $t$  as well. Hence, only the plate width  $b$  is a variable factor which is changed to achieve the different length-to-width ratios. To obtain a computation related as close to reality as possible, the time to traverse this Mach number range is deduced from the Saturn V trajectory and set to  $T = 10$ . The chosen start conditions and resulting differences are presented

in table 5.4. Note that the dynamic pressure of the trajectories is set to constant

**Table 5.4:** Initial values of the trajectories with identical travel time and distances of the stability boundary in Mach number and dynamical pressure

$a/b$	$M$	$\Delta M$	$\lambda$	$\Delta\lambda$	percentage dev.
0	1.6	0.2	498.83	94.83	23.47
0.5714	1.6	0.2	568.44	110.24	24.06
1	1.6	0.2	720.08	140.08	24.15
1.75	1.6	0.2	1246.58	228.58	22.45

to facilitate obtaining similar trajectory conditions. Therefore  $\lambda$  has to match the critical pressure at  $M = 1.8$ . It can be seen that the percentage deviation of the dynamic pressure to the critical value is relatively conform. Thus, it can be assumed that the parameters are equal (relatively, not quantitatively) for each panel. This assumption proves to be true by regarding Figs. 5.24 a to d. Herein the deflections

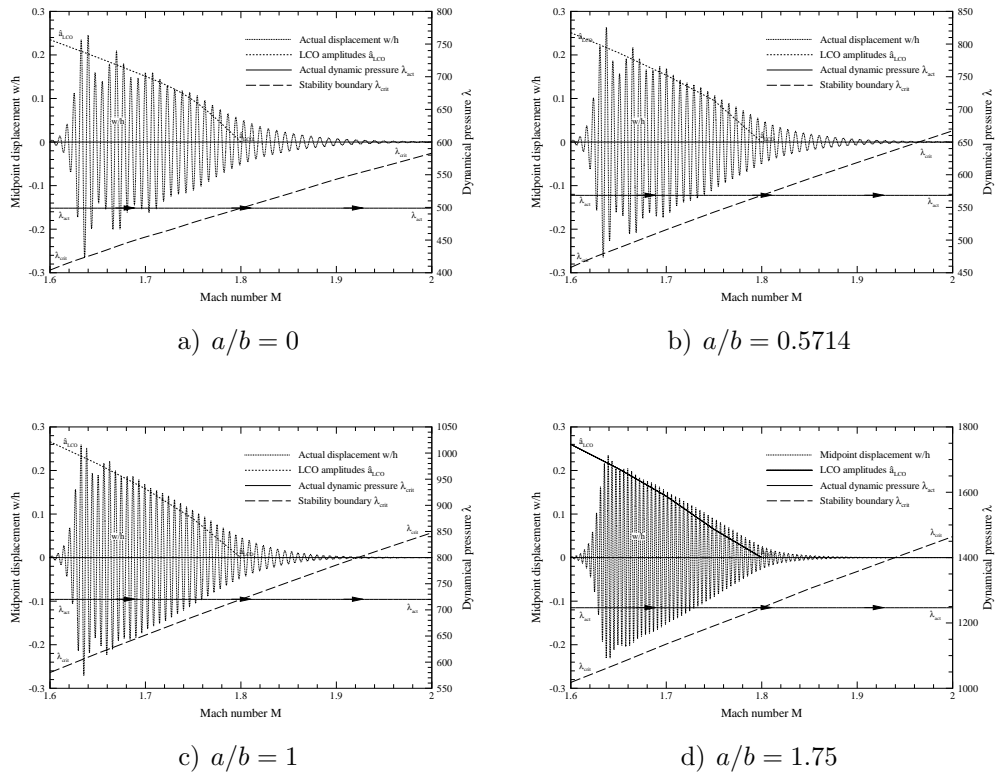


**Figure 5.24:** Trajectories beginning at similar distance in the dynamic pressure and Mach number from the stability boundary for different length-to-width ratios.



of the four panels are presented and compared with the LCO-amplitudes from the steady computations. It can be seen that the curves are very conform and scarcely deviate from one another. All four show the typically observed behaviour of a fast increase followed by a slow drop after the LCO deflections decrease. The curves only differ slightly in their magnitude and due to some outlier of the amplitudes, which are likely to be caused by the short travel time and complex oscillations in this post-critical region. These results suggests that the panel geometry scarcely influences the behavior of the trajectory. This outcome is reasonable. The influence of the length-to-width ratio (presented in chapter 5.3.2) shows that the resulting amplitudes for different panels exposed to flow conditions in a similar manner above the stability boundary exhibit the same amplitudes. Hence, it is not surprising that the shown computations yield very conform deformations. Furthermore it can be concluded that a panel, even if exhibiting a higher pressure, shows the same reaction crossing the stability boundary at comparable start conditions.

#### 5.4.8 Trajectories affected by different participating modes

In chapter 5.3.1 it was observed that within the Mach number regions from 1.3 to 1.7 higher modes contribute to the flutter motion. To investigate trajectories exhibiting these effects two computations have been carried out for the same panel and travel time within this region (Traj. D1 and E1 from Fig. 5.17). The first outcome (5.25) is obtained by computing trajectory D1, which enters the region of the higher participating modes only slightly above the (manually identified) flutter boundary. The resulting displacements correspond to the results of the computation of the trajectory starting at  $\lambda_0 = 1.5\lambda_{crit,0}^*$  (Fig. 5.21 c) and show further agreement to the first two presented trajectory computations (Figs. 5.18 and 5.19). The deflections of the panel traveling along the trajectory show a rapid increase until reaching the LCO amplitude and then exhibit a delay to the dropping extreme deflections of the steady computations. The flutter boundary, obtained by including the contributions of the higher modes (discussed in chapter 5.3.1), is presented as a dashed-dotted line. Thus, the point at which the panel enters the region in which higher modes contribute can be seen. However, the motion of the panel does not show any influence and even drops to zero before crossing the lower stability boundary. In the steady computations it was observed that the observed mode shapes in this region establish very slowly. The dynamic pressures during the trajectory  $\lambda_{traj}$

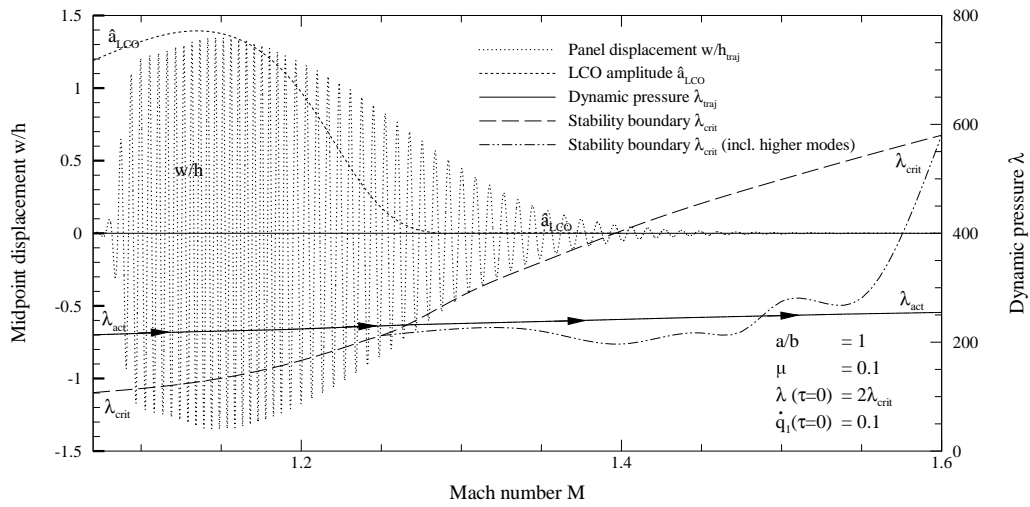


**Figure 5.25:** Trajectory crossing the stability boundary for a squared panel slightly entering the region with higher participating modes.

assume values scarcely above the critical ones and therefore the oscillations observed in these regions may not be able to settle. Regarding the actual dynamic pressure of the second trajectory (Fig. 5.26) for the squared plate in contrast, the panel travels through this regions with a dynamic pressure substantial above the flutter boundary. These circumstances are reflected in the motion of the panel. For the

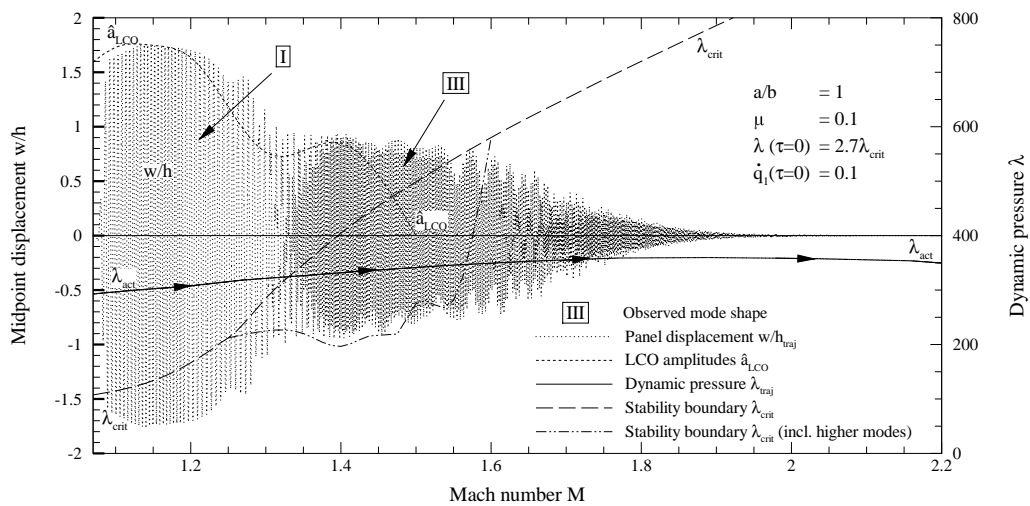


**Figure 5.26:** Trajectory crossing the stability boundary for a squared panel entering the region with higher participating modes.

---

trajectory with the higher dynamic pressures the deflection of the panel shows analogue to the previous computation a fast increase and then a delayed decay. When the actual Mach number reaches the ranges of the higher participating modes, the observed motion changes to an oscillation with a higher frequency and exhibits the shape mainly influenced by the third natural plate mode. This indicates that a panel traversing the region of the more complicated mode participation shows an influence of these higher modes in its flutter motion. However, these influences arise only for a difference in the dynamic pressure of a magnitude for which the arising mode shapes can settle fast enough. Comparing the delays of both trajectories, the latter exhibits a faster growth after the excitation and even seems to adapt faster for the decay phase of the first oscillation shape. The latter establishing oscillation on the other hands shows a much larger delay. However, this comparison does not seem very fertile due to the high differences in the panel motion of the two trajectories.

# 6 Summary and outlook

## 6.1 Summary

The current work focuses on two parts. On the one hand the influences of several parameters on the flutter solution are regarded and on the other hand the effects of time variable flow conditions are analysed. Therefore the first part of the present work is a literature study about the influence of several parameters on the aeroelastic characteristics of flat plates exposed to a low supersonic flow. This study reveals that there is a lack of literature about the effects for Mach numbers smaller than 2. Furthermore it was realized that no detailed investigations were carried out with flow conditions which vary in time. To examine the stated subjects of interest, a code developed by Ventres[27] is enhanced to a temporal adjusting integrator to account for flow conditions which change according to a chosen trajectory. Furthermore, a feature is added to parse an input file for the influencing parameters and computational settings. To facilitate easy and user-friendly investigations the post-processing is improved and additional functionalities enabling automatic analyses have been integrated. The validation by comparisons with examples from the literature show good agreements for the stability boundaries as well as post-critical flutter characteristics. A parameter study was conducted about the influencing parameters based on the literature study yielding the following conclusions:

The Mach number has a strong influence on the complete flutter behaviour. On the one hand it effects the magnitude of stability boundary and very low critical dynamic pressures have been observed for small supersonic Mach numbers from 1 to circa 1.4. Further this parameter changes the shape of the flutter oscillation which would arise for dynamic pressures above the stability boundary. Even the magnitude of the occurring panel displacements in the unstable regions depend heavily on

the Mach number.

The length-to-width ratio mainly influences the critical values, at which flutter begins to occur. It has been observed that an increase in the plate length strongly raises the critical dynamic pressure. Computations of unstable systems show that the length-to-width ratio has no significant influence on the deformations of the panel after flutter arises.

A comparison of pinned and clamped panels shows that the stability boundary can be significantly increased if the panel is completely constraint.

During all computations within the Mach number range of 1.3 and 1.8 and values of the length-to-width ratio between 0 and 2 higher natural modes have been observed contributing to the flutter solution. Because of these influences the stability boundary was found to be reduced.

The newly integrated tool to compute time variable flow conditions is used to simulate flat panels flying along trajectories analogue to the flow conditions of a launch of a Saturn V rocket. Several trajectories, summarized in Fig. 5.17, have been simulated and lead to the following outcome:

The computations of different trajectories show that the arising motion grows rapidly towards the magnitude of infinite long computations with constant flow conditions. After crossing the flutter boundary the panels show a delay in the decrease of the plate motion.

The closer the trajectories approach the flutter boundary the smaller are the obtained amplitudes and the danger of excitation of higher modes.

Investigations of identical panels and trajectories given different times to travel through a specific range of Mach numbers show that the observed delay relies heavily on the time taken to traverse a trajectory.

Further computations of panels with different length-to-width ratios following comparable trajectories show that the behaviour is very similar for different geometries. A variation of the trajectory path and hence different dynamic pressures for an identical panel showed that the resulting plate motion and the arising delay is distinct for each trajectory.

## 6.2 Outlook

The obtained results yield numerous cause and possibilities for further investigations. Firstly, not all parameters which have an influence on flutter of panels have been part of this work. The presented software can for example be used to examine the influence of the density ratio (of the fluid and the panel), the effects of cavities or the influence of external stresses due to thermal differences. The results of this study offer cause for further investigation on the one hand and verification on the other hand. Especially the observed region of increased modal participation has to be inspected by further investigations applying different theoretical techniques or experiments. The complete range of investigations with time variable computations has not been performed in a similar manner and has to be verified by experimental techniques and further analyses. Additionally many more computations could be carried out among others focusing on different types of trajectories, i.e. 'vertical' traverses of the flutter boundary. Furthermore the software can be extended even more especially for the post-critical investigations.

# Bibliography

- [1] A. R. Collar. The expanding domain of aeroelasticity. *Journal of the Royal Aeronautical Society*, L:613–636, 1946.
- [2] I. E. Garrick. Nonsteady wing characteristics. In *High Speed Aerodynamics and Jet Propulsion*, volume 2, chapter F. Princeton University Press, 1957.
- [3] Maurice A. Sylvester and John E. Baker. Some experimental studies of panel flutter at mach number 1.3. Technical report, National Advisory Committee for Aeronautics (NACA), February 1957.
- [4] Wallace D. Hayes. A buckled plate in a supersonic stream. Technical report, North American Aviation, Inc., May 1950.
- [5] John W. Miles. Dynamic chordwise stability at supersonic speeds. Technical report, North American Aviation, Inc., October 1950.
- [6] Joe Griffin Eisley. *Panel Flutter in Supersonic Flow*. PhD thesis, California Institute of Technology, Pasadena, California, 1956.
- [7] John Mills Hedgepeth. Flutter of rectangular simply supported panels at high supersonic speeds. Master’s thesis, Virginia Polytechnic Institute, March 1957.
- [8] Maurice A. Sylvester, Herbert C. Nelson, and Herbert J. Cunningham. Experimental and theoretical studies of panel flutter. Technical report, National Advisory Committee for Aeronautics (NACA), 1955.
- [9] M.H. Lock and Y.C. Fung. Comparative experimental and theoretical studies of the flutter of flat panels in a low supersonic flow. Technical report, California Institute of Technologie, Pasadena, 1961.
- [10] Earl H. Dowell. Theoretical and experimental panel flutter studies in the mach number range 1.0 to 5.0. *AIAA Journal*, 3(12):2292 – 2304, October 1965.

- 
- [11] Herbert C. Nelson and Herbert J. Cunningham. Theoretical investigation of flutter of two-dimensional flat panels with one surface exposed to supersonic potential flow. Technical report, National Advisory Committee for Aeronautics, 1956.
- [12] Earl H Dowell. Nonlinear oscillations of a fluttering plate ii. *AIAA Journal*, 5, No. 10:1856 – 1862, 1967.
- [13] Earl H Dowell. Generalized aerodynamic forces on a flexible plate undergoing transient motion. *Quarterly of Applied Mathematics*, 24(4):331 – 338, 1967.
- [14] Jack J. McNamara and Pretz P. Friedmann. Aeroelastic and aerothermoelastic analysis of hypersonic vehicles: Current status and future trends. In *ASC Structures, Structural Dynamics, and Materials Conference*, 2007.
- [15] Lado Jr. Muhlstein, Peter A. Jr. Gaspers, and Dennis W. Riddle. An experimental study of the influence of the turbulent boundary layer on panel flutter. Technical report, National Aeronautics and Space Administration (NASA), 1968.
- [16] Jr. Muhlstein, L. Experimental evaluation of the aerodynamic damping of skin panels at low supersonic mach numbers. In *13th Structures, Structural Dynamics, and Materials Conference*, 1972.
- [17] Oddvar O. Bendiksen and Gary A. Davis. Nonlinear traveling wave flutter of panels in transonic flow. In *36th AIAA/ASME/ASCUA/HSIASC Structures, Structural Dynamics and Materials Conference*, 1995.
- [18] Raymond E. Gordnier and Miguel R. Visbal. Computation of three-dimensional nonlinear panel flutter. In *39th AIAA Aerospace Sciences Meeting & Exhibit*, 2001.
- [19] Raymond E. Gordnier and Miguel R. Visbal. Development of a three-dimensional viscous aeroelastic solver for nonlinear panel flutter. *Journal of Fluids and Structures*, 16(4):497 – 527, 2002.
- [20] Atsushi Hashimoto, Igor Men'Shov, and Yoshiaki Nakamura. Panel flutter analysis with a fluid-structure coupled scheme. In *33rd AIAA Fluid Dynamics Conference and Exhibit*, 2003.
- [21] Marko Alder. Development and validation of a fluid-structure solver for transonic panel flutter. *AIAA Journal*, 53(12):3509 – 3521, 2015.



- 
- [22] Earl H Dowell. A review of the aeroelastic stability of plates and shells. *AIAA Journal*, 8(3):385 – 399, March 1970.
- [23] J. H. Cunningham. Flutter analysis of flat rectangular panels based on three-dimensional supersonic potential flow. *AIAA Journal*, 1:1795 – 1801, 1963.
- [24] Earl H Dowell. *Aeroelasticity of plates and shells*. Number 1. Springer Science & Business Media, 1974.
- [25] Earl H Dowell. Nonlinear oscillations of a fluttering plate i. *AIAA Journal*, 4(7):1267 – 1275, July 1966.
- [26] John Dugundji. Theoretical considerations of panel flutter at high supersonic mach numbers. *AIAA Journal*, 4(7):1257 – 1266, July 1966.
- [27] Charles S. Ventres. *Nonlinear Flutter of Clamped Plates*. PhD thesis, Princeton University, October 1969.
- [28] G. T. Pinson. Apollo/saturn v postflight trajectory. NASA Rept. - AS-512, April 1973.
- [29] Atsushi Hashimoto and Takashi Aoyama. Effects of turbulent boundary layer on panel flutter. *AIAA Journal*, 47(12):2785–2791, December 2009.
- [30] P. Roache. Perspective: A method for uniform reporting of grid refinement studies. *Journal of Fluids Engineering*, 116(3):405–413, 1994.
- [31] G. A. Davis and O. O. Bendiksen. Transonic panle flutter. In *34th AIAA/ASME/ASCE/AHS/ASC Structures, Structural Dynamics and Materials Conference*, 1993.
- [32] M. Alder. Nonlinear dynamics of pre-stressed panels in low supersonic turbulent flow. *AIAA Journal*, in peer-review process, 2016.
- [33] Honghua Dai, Xiaokui Yue, Dan Xie, and Satya N. Atluri. Chaos and chaotic transients in an aeroelastic system. *Journal of Sound and Vibration*, 333:7267–7285, 2014.
- [34] Earl H. Dowell and T. Fang. Numerical simulations of periodic and chaotic responses in a stable duffing system. *International Journal of Non-Linear Mechanics*, 22:401–425, 1987.

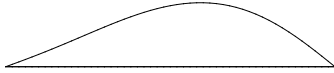
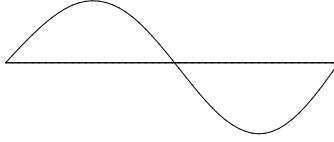
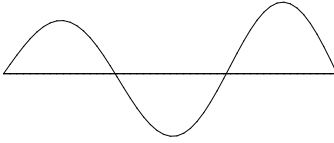
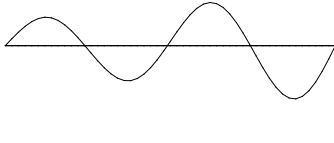
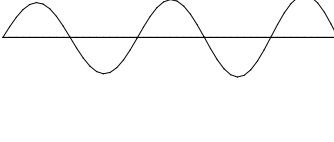
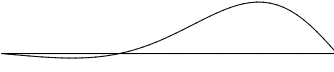
# A Saturn V trajectory

**Table A.1:** Time, non-dimensional time, Mach number, dynamic pressure, non-dimensional dynamic pressure of the Saturn V trajectory.[28]

<b>t [s]</b>	<b><math>\tau</math></b>	<b>M</b>	<b><math>p_{\text{dyn}} [\text{N/m}^2]</math></b>	<b><math>\lambda</math></b>
0	0.00	0.00	0.0000	0.00
5	7.34	0.02	0.0001	0.10
10	14.69	0.04	0.0005	0.37
15	22.03	0.12	0.0010	0.78
20	29.38	0.16	0.0017	1.41
25	36.72	0.22	0.0028	2.26
30	44.06	0.26	0.0041	3.38
35	51.41	0.32	0.0060	4.92
40	58.75	0.40	0.0085	6.97
45	66.10	0.48	0.0119	9.74
50	73.44	0.58	0.0154	12.61
55	80.79	0.71	0.0189	15.52
60	88.13	0.84	0.0226	18.55
65	95.47	1.00	0.0260	21.32
70	102.82	1.18	0.0290	23.78
75	110.16	1.36	0.0314	25.73
80	117.51	1.60	0.0330	27.06
85	124.85	1.82	0.0334	27.37
90	132.19	2.06	0.0301	24.70
95	139.54	2.30	0.0261	21.42
100	146.88	2.54	0.0223	18.25
105	154.23	2.80	0.0184	15.05
110	161.57	3.10	0.0145	11.89
115	168.91	3.40	0.0107	8.75
120	176.26	3.74	0.0078	6.36
125	183.60	4.06	0.0056	4.57
130	190.95	4.44	0.0040	3.28
135	198.29	4.84	0.0028	2.30
140	205.64	5.26	0.0020	1.62
145	212.98	5.72	0.0012	0.98
150	220.32	6.20	0.0007	0.55
155	227.67	6.80	0.0003	0.23
160	235.01	7.56	0.0001	0.06
165	242.36	8.60	0.0000	0.00

## B Observed mode shapes

Table B.1: Overview of the observed mode shapes.

No.	Observed mode shape
I	
II	
III	
IV	
V	
VI	

# C Example trajectory file for the 'TAIFUN' code

=====

Saturn V trajectory

=====

-

Fitted to cross the transonic

dip for a panel with  $a/b=0$

-

=====

tau	M	Lamda
0	1.07	18.74230633
13.19785979	1.13	19.22757453
26.39571958	1.19	19.59681818
39.59357937	1.27	20.38311946
52.79143916	1.35	20.89266651
65.98929894	1.44	21.50558806
79.18715873	1.54	22.08656532

92.38501852	1.65	22.587899
105.5828783	1.77	22.96844504
118.7807381	1.89	23.01862329
131.9785979	2.02	22.91490797
145.1764577	2.16	22.63611848
158.3743175	2.29	21.7964512
171.5721773	2.41	20.5505712
184.770037	2.52	19.06491992
197.9678968	2.63	17.58327571
211.1657566	2.75	16.24728325

## D Example input file for the 'TAIFUN' code

```
=====
-----{ Example input file }-----
=====
```

This is an example input file for the Taifun Software which includes all possible input statements and additional comments and explanations.

```
=====
                                Output settings
=====
```

The following statements include informations about the generall settings of the output.

```
-----
Output folder                = mode-1_cl
-----
```

Gives the name of the folder in which the solution files and logfiles are saved.

```
-----
Output to shell              = .true.
-----
```

-----  
Selects if the log of the input file parsing and the actual  
progress is plotted to the shell.  
-----

-----  
Output to file = .true.  
-----

Selects if the log of the input file parsing and the actual  
progress is plotted to a text file.  
-----

=====

=====

Parameter definitions

=====

In this section the parameters which are used for the  
computations can be defined. It is possible to input non-  
dimensional values or dimensioned values.

Non-Dimensional Values

=====

-----  
Mach number = 1.35  
-----

Defines the Mach number. Attention: Values smaller than 1  
can not be chosen.  
-----

-----  
Aspect ratio = 1  
-----

Defines the length-to-width ratio of the panel. For a two-

dimensional panel set a value close to zero but not equal to zero.

-----  
-----  
Lambda = 250  
-----

Defines the non-dimensional dynamic pressure.  
-----

-----  
Density ratio = 0.1  
-----

Defines the ratio of the density of the fluid and the structure.  
-----

-----  
Poisson ratio = 0.33  
-----

Defines the value of the poisson ratio  
-----

-----  
Number of modes = 12  
-----

Defines the number of modes which are included in the computation.  
-----

-----  
Stat. pressure diff = 0  
-----

Defines the difference of the static pressure.  
-----



-----  
Cavity pressure diff               = 0  
-----

Defines the difference of the pressure above the panel and  
the cavity below the panel.  
-----

-----  
Pre-stress Rx                       = 0  
-----

Defines the internal stress in the x-direction.  
-----

-----  
Pre-stress Ry                       = 0  
-----

Defines the internal stress in the y-direction.  
-----

-----  
Structural Damping                 = 0  
-----

Defines the value of the structural damping.  
-----

-----  
Delta tau                           = 0.001  
-----

Defines the size of the time step for the integration.  
-----

-----  
Max tau                              = 0.2  
-----

Defines the non-dimensional time at which the computation  
is stopped.

-----

-----

Boundary constraints = 'clamped'

-----

Selects if the panel is clamped or pinned on the edges.

-----

-----

Nonlinear = .true.

-----

Selects if nonlinearities are taken into account.

-----

-----

Zero edge displacement = .false.

-----

Selects if a zero edge displacement shall be included.

-----

-----

Set delta s = .false.

-----

Selects if the time step size s for the admittance fcn.  
shall be defined manually.

-----

-----

Set nr. of time steps = .false.

-----

Selects if the nr. of time steps for the admittance fcn.  
shall be defined manually.

-----

-----

Delta s = 0.001

-----  
Defines the time step size of the admittance functions.  
-----

-----  
Number of time steps           = 1000  
-----

-----  
Defines the nr. of time steps of the admittance functions.  
-----

-----  
Aerodynamic model               = 'potential'  
-----

-----  
Selects if the aerodynamics shall be modeled by the full  
linearised potential theory ('potential'), piston theory  
( 'piston') or no theory ('none').  
-----

-----  
Interpolate adm. fcn.           = .false.  
-----

-----  
Defines if the admittance functions shall be interpolated.  
If 'Set delta s' or 'Set nr. of time steps' is set to true  
this will automatically be done.  
-----

-----  
Interpolation type               = 'polynomic'  
-----

-----  
Selects if the admittance functions shall be interpolated by  
a linear interpolation ('linear') or by using the Lagrange  
interpolation ('polynomic').  
-----

-----  
Interpolation degree            = 3  
-----

-----  
Defines the degree of interpolation (nr. of used nodes) for  
the Lagrange interpolation.  
-----

-----  
Overwrite adm. fcn. = .false.  
-----

Selects if the original admittance functions shall be  
replaced within the output file.  
-----

Dimonsioned Values  
=====

-----  
Dimensioned values = .false.  
-----

Selects if dimensioned values are used as input or non-  
dimensional values.  
-----

-----  
Edge a = 0.875  
-----

Defines the length of the panel (streamwise direction).  
-----

-----  
Edge b = 0.875  
-----

Defines the width of the panel (normal direction).  
-----

-----  
Youngs modulus = 4.739  
-----

-----  
Defines the youngs modulus of the material.  
-----

-----  
Thickness = 1.0e-3  
-----

Defines the thickness of the panel.  
-----

-----  
Structure density = 2909.9  
-----

Defines the density of the material.  
-----

-----  
Fluid density = 0.7207  
-----

Defines the density of the fluid.  
-----

-----  
Pressure = 48355.0  
-----

Defines the pressure of the flow.  
-----

-----  
Isentropic exponent = 1.4  
-----

Defines the value of the isentropic exponent.  
-----

-----  
Gas constant = 287  
-----

-----  
Defines the value of the gas constant.  
-----

-----  
Fluid temperature                   = 233.75714885495  
-----

Defines the temperature of the fluid.  
-----

-----  
Initial conditions of the modes  
-----

The following statements define the initial values of the displacement and velocity of the modes in generalised coordinates. These inputs define the initial excitation.

Initial displ. (1)                   = 0  
Initial velocity (1)                 = 0  
Initial displ. (2)                   = 0  
Initial velocity (2)                 = 0  
Initial displ. (3)                   = 0  
Initial velocity (3)                 = 0  
Initial displ. (4)                   = 0  
Initial velocity (4)                 = 0  
Initial displ. (5)                   = 0  
Initial velocity (5)                 = 0  
Initial displ. (6)                   = 0  
Initial velocity (6)                 = 0  
Initial displ. (7)                   = 0  
Initial velocity (7)                 = 0  
Initial displ. (8)                   = 0  
Initial velocity (8)                 = 0  
Initial displ. (9)                   = 0  
Initial velocity (9)                 = 0

Initial displ. (10) = 0  
Initial velocity (10) = 0  
Initial displ. (11) = 0  
Initial velocity (11) = 0  
Initial displ. (12) = 0  
Initial velocity (12) = 0

-----  
=====  
=====

Iteration

=====  
This section defines the settings of the automatic iteration.

-----  
Iteration status = .false.

-----  
Selects if a automatic iteration is executed or not.  
-----

-----  
Iteration parameter = Lambda

-----  
Selects the parameter which is iterated. Possible choices are all numerical variables which can be defined in the non-dimensional parameter or dimensioned parameter section. The entered parameter has to match the identifier which can be seen above. The value which is given in the parameter definition is used as start value.  
-----

-----  
Iteration increment = 5  
-----

Defines the increment of the iteration.

-----  
-----  
Multiplication = .false.

-----  
Selects if the values are multiplied or added by the iteration increment.

-----  
Iteration limit = 550

-----  
Defines the limit up to which the iteratio is carried out.

=====  
=====  
Solution analysis

=====  
The following statements adjust the settings of the automatic analysis of the solution.

-----  
Analyse solution = .false.

-----  
Selects if the automatic analysis shall be executed.

-----  
Analyse sol. at point = 2

-----  
Selects the point of the plate which is to be analized.  
The entered nr. corresponds to the column of the solution



file starting at the first column presenting deformations of the panel.

-----  
-----  
Compare slopes = .false.

-----  
Selects if the amplitudes are determined by comparing the slopes of the oscillation or for '.false.' by comparing the actual values from the solution file.

-----  
-----  
No. of values to comp. = 5

-----  
Defines the nr of slopes which are compared.

-----  
-----  
Min. stable amplitudes = 100

-----  
Defines the nr of amplitudes which have to be stable to declare an oscillation as sustained.

-----  
-----  
Max. adjustment steps = 50

-----  
Defines the nr of adjustment steps after which the automatic identification of the crit. value is cancelled.

-----  
-----  
Max. allowed deviation = 0.0005

-----  
Defines the range in which the growth of the mean amplitude

is regarded as stable.

-----  
-----  
Max. amp. fluctuation = 0.001

-----  
Defines the range in which the differences of the amplitudes are regarded as stable.

-----  
Start analyse at tau = 15

-----  
Sets the non-dimensional time after which the program tries to identify the state of the oscillation.

-----  
Skip until tau = 5

-----  
This value enables to exclude the first part of the solution up to the entered non-dimensional time from the analysis.

-----  
Nr. of skipped amp. = 0

-----  
Defines the nr. of amplitudes (beginning after the skipped time period) which are excluded from the analysis.

-----  
Start 1st attempt at = 5

-----  
Defines the minimum nr. of amplitude which is needed to start the first analysis attempt. The first attempt compares

all local log. decrements of the maxima.

-----  
-----  
Start 2nd attempt at           = 10  
-----

Defines the minimum nr. of amplitude which is needed to start the second analysis attempt. The second attempt checks if the main nr. of local log. decrements is positiv, negative or zero.

-----  
-----  
Start 3rd attempt at           = 15  
-----

Defines the minimum nr. of amplitude which is needed to start the second analysis attempt. The thrid attempt compares the mean log. decrement with the growth between the mean amplitude of the first and second half.

-----  
-----  
Stop analysis at               = 500  
-----

Defines the nr. of amplitudes after which the automatic analysis is aborted.

-----  
-----  
Analysis increment             = 500  
-----

Defines the increment nr. of time steps in which the program tries to analyse the oscillation.

Automatic identification of critical value

=====

-----  
Automatic adjustment = .true.

-----  
Selects if the automatic identification of the critical value is carried out by the program.  
-----

-----  
Adjustment parameter = Lambda

-----  
Selects for which parameter the crit. value shall be identified. Possible choices are all numerical parameters from the parameter definition.  
-----

-----  
Lower range value = 485

-----  
Defines the lower boundary value which borders the range in which the crit. value is searched.  
-----

-----  
Upper range value = 500

-----  
Defines the upper boundary value which borders the range in which the crit. value is searched.  
-----

-----  
Expand upper range by = 10

-----  
Defines the increment with which the upper range value is

increased if the upper range value yields a excited oscillation.

-----  
-----  
Keep interim solutions = .true.

-----  
Selects if the solutions of the computed values shall be kept after it is analised.

-----  
Range precision = 0.5

-----  
Defines the precision in which the crit. value is located.

=====  
Trajectory options

=====  
The following statements are used to adjust the computation of the time variable flow conditions.

-----  
Compute trajectory = .false.

-----  
Selects if the parameters Mach number and dynamic pressure shall be varied during the computation according to a trajecotry file.

Trajectory file = tconst\_ab1.traj

-----  
Defines the name of the file containing the trajectory as  
a tabel.  
-----

-----  
1st line of data = 6  
-----

-----  
Defines the line of the trajectory file at which the  
programm starts to read in the values of the parameters.  
-----

-----  
Polyn. interpolation = .true.  
-----

-----  
Selects if the values of the variable parameters for the  
actual time step shall be interpolatet by using the lagrange  
interpolation ('.true.') or by a linear interpolation.  
-----

=====  
-----  
Plot Options  
-----

In this section the possible output can be determined.  
-----

Plot solution = .true.  
-----

-----  
Selects if the displacements and velocieties are plotted.  
-----

-----  
Plot surface solution           = .true.  
-----

Selects if the grid simulating the surface deformations  
is plotted.  
-----

-----  
Plot adm. fcn.                   = .false.  
-----

Selects if the admittance functions are plotted.  
-----

-----  
Plot B                           = .false.  
-----

Selects if the B matrix is plotted.  
-----

-----  
Plot amplitudes                 = .false.  
-----

Selects if the identified amplitudes are plotted.  
-----

-----  
Plot results                    = .false.  
-----

Selects if the identified crit. values are plotted.  
-----

-----  
Write tecplot header           = .true.  
-----

Selects if a header containing informations for Tecplot360  
is plotted as first row of the solution files.

-----

-----

Plot points = 3

-----

Determines the numbers of points along the plate length for which the panel deformations and velocities are computed.

-----

-----

Plot modal particip. = .false.

-----

Selects if the fractions of the participating modes is plotted in the solution file.

-----

Surface Deformations  
=====

-----

Surface plot period = 1

-----

Defines the increment in which the surface deformations are plotted.

-----

-----

Start surface solution = 0

-----

Defines the time point from which onwards the surface deformations are plotted.

-----

-----

No. of elements in x = 50



-----  
Defines the points in x-direction and thus the resolution  
of the grid.  
-----

-----  
No. of elements in y            = 50  
-----

Defines the points in y-direction and thus the resolution  
of the grid.  
-----

-----  
Scaling                            = 1  
-----

Defines the factor by which the surface deformations are  
scaled in the output file.  
-----

-----  
No. of plot periods               = 1  
-----

Defines the number of plot periods for the surface displ.  
-----

Definition of the plot periods  
-----

Start surface plot(1)            = 0  
End surface plot(1)              = 0.01  
Start surface plot(2)            = 10  
End surface plot(2)              = 10.1  
Start surface plot(3)            = 25  
End surface plot(3)              = 25.1  
Start surface plot(4)            = 50  
End surface plot(4)              = 50.1

=====